Journal of Petroleum Science and Engineering 216 (2022) 110823

Contents lists available at ScienceDirect

Journal of Petroleum Science and Engineering

journal homepage: www.elsevier.com/locate/petrol

Geological characteristics and shale oil potential of alkaline lacustrine source rock in Fengcheng Formation of the Mahu Sag, Junggar Basin, Western China

Yuping Wu [a,b], Chenglin Liu [a,b,*], Fujie Jiang [a,b,**], Tao Hu [a,b,***], Jiahao Lv [a,b], Chenxi Zhang [a,b], Xuguang Guo [c], Liliang Huang [c], Meiling Hu [a,b], Renda Huang [a,b], Rizwan Sarwar Awan [a,b], Yi Zhao [c]

[a] State Key Laboratory of Petroleum Resources and Prospecting, China University of Petroleum, Beijing, 102249, China
[b] College of Geosciences, China University of Petroleum, Beijing, 102249, China
[c] Research Institute of Exploration and Development, PetroChina Xinjiang Oilfield Company, Karamay, 834000, China

ARTICLE INFO

Keywords:
Alkaline lacustrine source rock
Shale oil potential
Fengcheng formation
Mahu sag

ABSTRACT

Shale oil is the main field of unconventional hydrocarbon exploration and exploitation. Additionally, deep (>4500 m) petroleum exploration in sedimentary basins is a worldwide frontier topic. The Fengcheng Formation in the Junggar Basin is deeply buried and formed in the special sedimentary environment of alkaline lakes. Studying this set of source rocks will provide insights into the deep unconventional hydrocarbon exploration in other basins with similar geologic settings worldwide. Therefore, this research takes Fengcheng shale as the object to systematically analyze the geochemical characteristics, reservoir quality, and shale oil resources' potential based on total organic carbon (TOC), Rock-Eval pyrolysis, vitrinite reflectance (R_o), X-ray diffraction (XRD), field emission-scanning electron microscopy (FE-SEM), and other experimental methods.

The Fengcheng shale has moderate organic matter abundance (0.5%–2.0%) and high hydrocarbon generation potential (averaging 3.95 mg/g). The shale is mainly comprised of type II kerogen, which can easily generate oil. Meanwhile, the source rock has reached the mature to high-mature thermal evolution stage. The mineral composition reveals the shale of Fengcheng Formation mainly contains higher values of carbonate minerals and lower quantities of clay minerals. Shale has poor physical properties, with porosity ranging from 1.0 to 12.0% (3.37% on average) and permeability generally lower than 0.1mD. However, the Fengcheng shale has a significantly higher brittleness than the North American marine shales and has good conditions for hydraulic fracturing. The pores developed in the shale are mainly intergranular, micro-fractures, and intragranular pores, while organic pores are rare. Generally, the hydrocarbon of the shale mainly exists in inorganic pores. Fractures are well developed in shale, and many micro-fractures and macro-fractures can be seen in the core. These fractures are important for hydrocarbons migration and accumulation. The shale oil saturation index OSI and S_1 show that despite the migration of some hydrocarbons from the source rocks of the Fengcheng Formation, a large amount of crude oil is still retained, and a considerable part of the shale oil is movable oil. It indicates that Fengcheng shale is rich in shale oil resources and is a favorable target for shale oil exploration and exploitation.

1. Introduction

Global unconventional resources are receiving great attention and have become an essential part of global oil and gas resources due to the continuous increase in energy demand and the continuous depletion of conventional resources (Hu et al., 2021a; Jarvie, 2012; Li et al., 2016; Zou, 2012). The success of the North American shale oil and gas has inspired exploration activities in other countries (Hu et al., 2020; Jarvie,

* Corresponding author. State Key Laboratory of Petroleum Resources and Prospecting, China University of Petroleum, Beijing, 102249, China.
** Corresponding author. State Key Laboratory of Petroleum Resources and Prospecting, China University of Petroleum, Beijing, 102249, China.
*** Corresponding author. State Key Laboratory of Petroleum Resources and Prospecting, China University of Petroleum, Beijing, 102249, China.
E-mail addresses: liucl@cup.edu.cn (C. Liu), jiangfj@cup.edu.cn (F. Jiang), thu@cup.edu.cn (T. Hu).

https://doi.org/10.1016/j.petrol.2022.110823
Received 23 September 2021; Received in revised form 30 May 2022; Accepted 28 June 2022
Available online 2 July 2022

2012; Zhao et al., 2020a). Countries such as Russia, Australia, and Argentina have begun shale oil research and exploration. In China, organic-rich shales are widely distributed, providing the necessary material conditions for shale oil formation (Zhao et al., 2020b; Zou, 2012; Zou et al., 2019). In 2019, the Ministry of Natural Resources of China initially calculated the geological resources of shale oil to be 283×10^8 tons. However, China's shale oil mainly occurs in lacustrine shale deposits. Its geological characteristics and distribution patterns are different from North American marine shales (Zhao et al., 2020b; Zou et al., 2019). The lacustrine shale systems are characterized by strong heterogeneity and high clay mineral content (Jin et al., 2021; Katz and Lin, 2014; Zhao et al., 2020a). Despite this, China has still carried out a large number of key research and industrial experiments in the major formations in various basins such as the Chang 7 Member (Ordos Basin), the Qingshankou Formation (Songliao Basin), the Lucaogou Formation (Junggar Basin), and the Shahejie Formation (Bohai Bay Basin). Exploration practice has proved that China's continental shale strata not only have the geological basis for the formation of abundant shale oil but also have the conditions for large-scale industrial exploitation (Hu et al., 2020; Huang et al., 2021; Jin et al., 2021; Li et al., 2019; Zhao et al., 2021).

The Junggar Basin is an important oil-producing basin in China, and the Mahu Sag is one of the hydrocarbon-rich sags in the basin (Hu et al., 2016; Liang et al., 2020; Liu et al., 2016). The petroleum exploration activities in this sag indicate the Fengcheng Formation (P_1f) provides a large number of petroleum resources for conventional oil and gas reservoirs (Feng et al., 2020; Liu et al., 2016). In recent years, the sag is undergoing shale oil exploration and research because the significant shale oil potential is still poorly understood. PetroChina Xinjiang Oilfield successively deployed FC1, BQ1, AK1, and MY1 wells to explore the potential of shale oil. The most important well MY1 was drilled in 2019 and obtained high-yield oil production. Till March 2021, the MY1 well has accumulated more than 500 days of production, and the accumulated oil production has exceeded 1.0×10^4 tons. However, the detailed shale oil potential of the P_1f shale in the Junggar Basin has not been completed to date in any of the previous literature. Previous studies

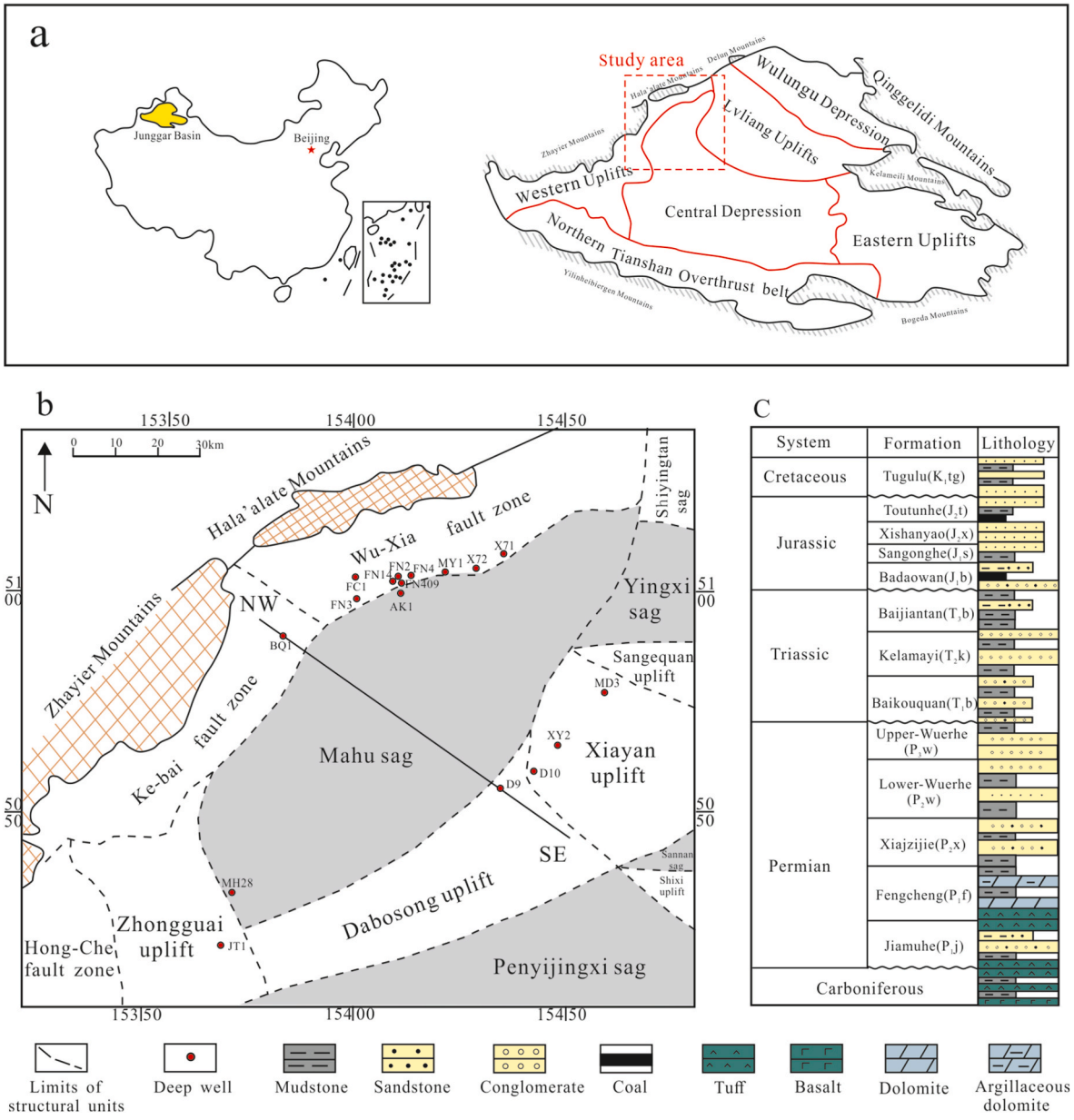

Fig. 1. (a) The location and structural units of the Junggar Basin; (b) The location of structural units and wells in the Mahu Sag; (c) The stratigraphic section in the Mahu Sag (after Cao et al., 2020; Xia et al., 2020).

mainly focused on the geochemical characteristics (Cao et al., 2015; Feng et al., 2020; Tao et al., 2019; Yu et al., 2018a, 2018b) and paleo-sedimentary environment (Cao et al., 2020; Wang et al., 2021; Yu et al., 2019; Zhang et al., 2018b) of the P_1f shale. As is well known, oil content and reservoir quality, in addition to the geochemical properties of source rock, are critical for the successful exploitation of shale oil. However, the quality of reservoirs, oil-bearing property, and shale oil resource potential of P_1f has not been thoroughly and systematically evaluated, which seriously affects the selection of targets for shale oil sweet spots. Furthermore, there is a lack of understanding of the P_1f shale characteristic in comparison to other well-known shales around the world. Therefore, the research objectives of this paper are: (1) To analyze the geochemical characteristics and the hydrocarbon generation potential of the P_1f shale; (2) To clarify the petrophysical properties and the oil-bearing characteristics of the shale; (3) To evaluate the shale oil resource potential of P_1f shale. This research is projected to fill a data gap in the Junggar Basin, allowing for more successful shale oil exploration and resource evaluation.

2. Geologic settings

The Junggar Basin is one of the most well-known basins in western China, with an area of about $13 \times 10^4 km^2$ (Fig. 1a). (Tang et al., 2021; Tao et al., 2019; Xia et al., 2020). Additionally, it is also a large and upper Paleozoic, Mesozoic, and Cenozoic superimposed basin, which has plentiful petroleum resources (Liang et al., 2020; Yu et al., 2018b, 2019). So far, industrial petroleum has been found in Paleozoic, Mesozoic, and Cenozoic strata (Cao et al., 2020; Zhi et al., 2019). The basin consists of six tectonic units (Yang et al., 2004), and the bulk of the basin lies in the Central Depression (Fig. 1B). Mahu Sag is situated in the northwest of the Central Depression with an area of 5000 km^2 (Feng et al., 2020). Its western side is adjacent to the Fault Zone, while the southwestern side is connected with the Zhongguai Uplift. In contrast, the Dabasong Uplift and Xiayan Uplift are distributed on the southeastern side, and the Shiyingtan Uplift is on the north (Cao et al., 2015; Zhi et al., 2021). There are several sets of effective source rocks in the sag (Fig. 1C) (Cao et al., 2015; Zhang et al., 2018a). Among them, the P_1f is the most important source of rocks for the formation of the huge oilfield in the northwestern margin of the basin (Feng et al., 2020; Hu et al., 2016; Xia et al., 2020; Zhang et al., 2018a).

2.1. Tectonic characteristics

The Mahu Sag was developed in the basement of the Late Carboniferous arc-basin system. It is overlaid by the Permian, Mesozoic, and Cenozoic terrestrial sediments (He et al., 2018; Imin et al., 2020; Tang et al., 2021). At present, the structural direction of the depression is mainly along NE-SW, showing a monoclinic dip in the southeast direction (Fig. 2) (Feng et al., 2020; Tang et al., 2021). However, during the geological period, the Mahu Sag has experienced different stages of tectonic evolution (Feng et al., 2020; He et al., 2018).

In the Early Carboniferous, the ancient Junggar ocean basin closed, forming a back-arc foreland basin (He et al., 2018; Imin et al., 2020; Liang et al., 2020; Tao et al., 2019). The Upper Carboniferous, Jiamuhe, and Fengcheng Formations were deposited from the Late Carboniferous to the Permian. Later, during Late Permian-Late Triassic, the thrusting activity in the basin was strongly active (He et al., 2018; Liang et al., 2020; Zhang et al., 2018a). Meanwhile, there are apparent unconformities between the Triassic strata and the underlying strata (He et al., 2018; Imin et al., 2020). During the Triassic, the Mahu Sag gradually evolved into a large intracratonic depression (He et al., 2018), and at the end of the Triassic, compression tectonic events caused uplift and denudation, forming an unconformity between Jurassic sediments and underlying strata (Imin et al., 2020). From Jurassic to Cretaceous, the deposits spread to the piedmont area, and the early thrust nappe was buried.

2.2. Sedimentary setting

The deposition of the Mahu Sag occurred in the asymmetric foreland basin. The basin's structure controlled the deposition of the Mahu Sag and the division of the Fengcheng Formation environment (Yu et al., 2019). The study area was a marine sedimentary setting in Carboniferous, mainly deposited a set of volcanic clastic rocks and tuffaceous rocks (Feng et al., 2020; Yu et al., 2018b). In the Early Permian, it was transformed into a closed to the semi-closed lacustrine depositional environment, and a set of carbonate-bearing shale (P_1f) was deposited. This set of strata is formed in a semi-deep to deep alkaline lake environment (Cao et al., 2015, 2020; Yu et al., 2019). Evidence of alkaline lakes includes the presence of alkali minerals, including wegscheiderite, shortite, trona, nahcolite, etc. (Cao et al., 2015, 2020; Xia et al., 2020). Previous studies have divided the sedimentary evolution of the P_1f into five stages (Cao et al., 2015; Xia et al., 2020; Zhang et al., 2018b). It is the same as the evolutionary stage of most alkaline lakes and alkaline deposits in the world, and similar sedimentary assemblages usually develop (Cao et al., 2015). The stratigraphic deposits of the P_1f have a continuous evolutionary process, and the lower part of the P_1f corresponds to the early onset preliminary stages. The middle part

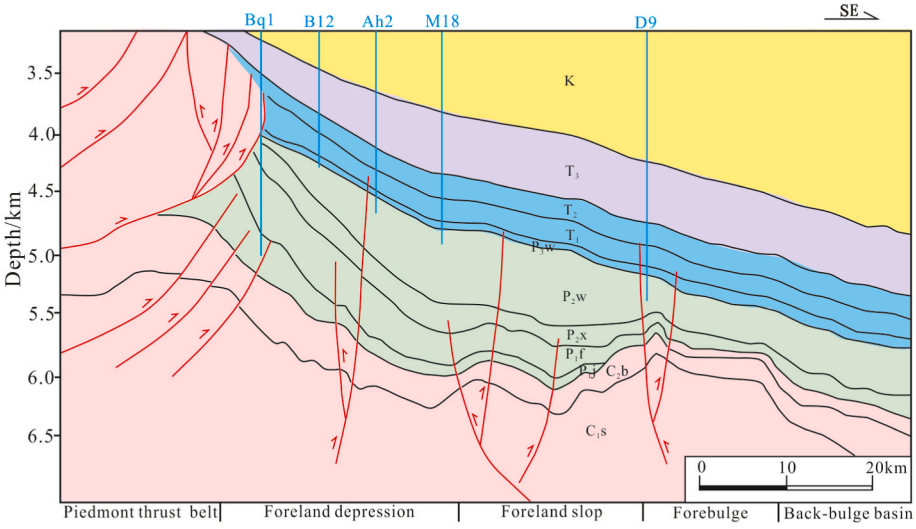

Fig. 2. Stratigraphic profiles across the Mahu Sag (from the Bq 1 Well to the D 9 Well) (after Imin et al., 2020).

corresponds to the third stage of the evolution of alkaline lakes (strong alkalinity forming stage) and appears with a lot of alkaline minerals. The upper part of the P_1f corresponds to the last two stages of the evolution of alkali lakes (weak and terminal alkalinity stages) (Zhang et al., 2018b).

2.3. Lithologic characteristics of the Fengcheng Formation

The Lower Permian P_1f consists mainly of mixed fine-grained sediments under the geological setting of deep to semi-deep lakes, with a thickness of 800–1800 m, and the overall trend is gradually thinning eastward (Li et al., 2021; Wang et al., 2021; Yu et al., 2019). The lithology of the P_1f is extremely complex, with mudstone, dolomite, limestone, sandstone, conglomerate, tuffaceous rocks, and volcanic rocks developed (Liang et al., 2020; Yu et al., 2019; Zhang et al., 2018a; Zhi et al., 2021). Different lithologies are frequently interbedded vertically, as shown in Fig. 3. According to the characteristics of lithological associations and sedimentary, the P_1f can be further divided into three informal members. The characteristics of each member are as follows:

2.3.1. P_1f_3

The thickness of P_1f_3 varies between 100 m and 300 m. It consists of

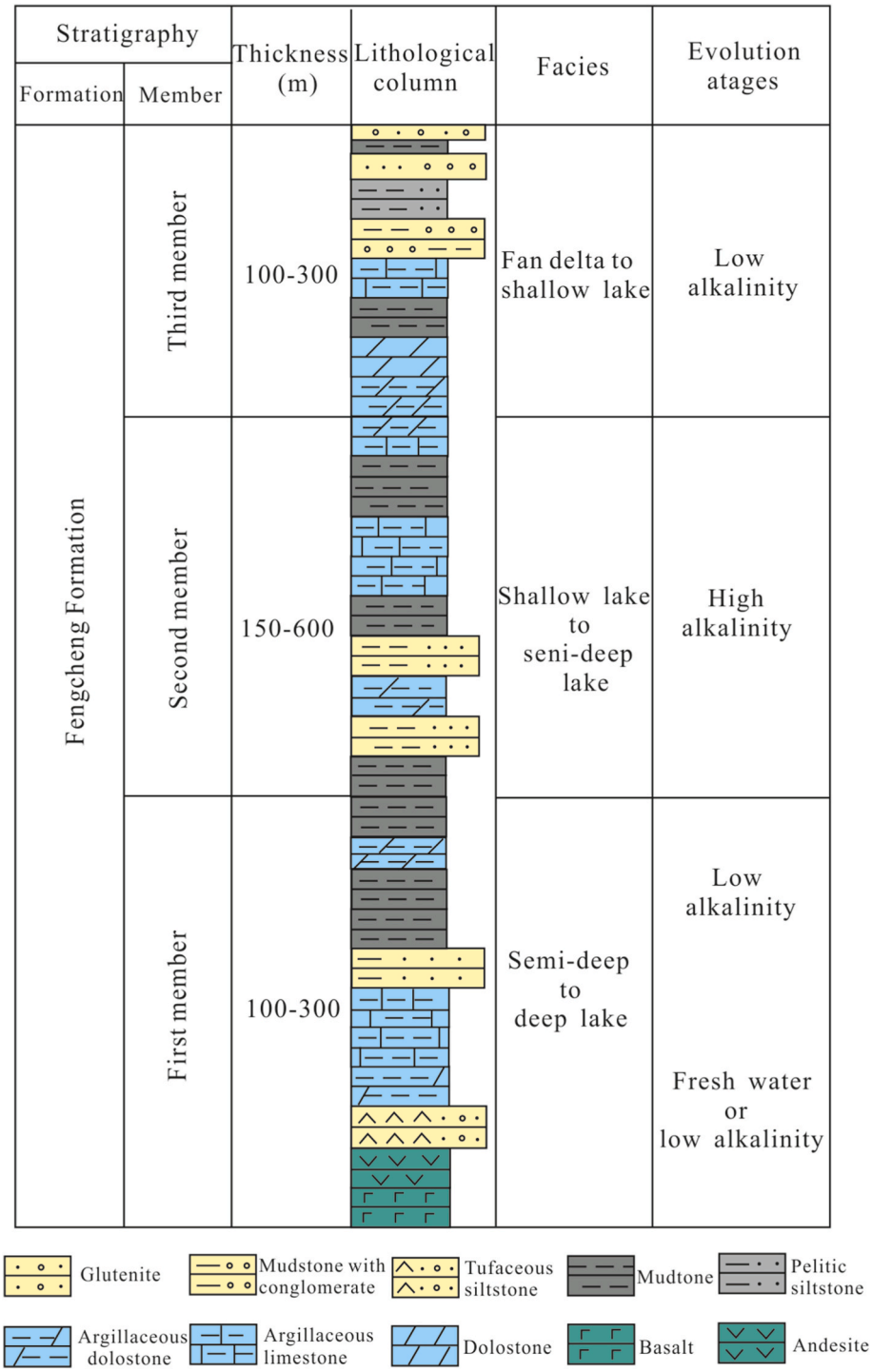

Fig. 3. The P_1f stratigraphy column and sedimentary evolution in the Mahu Sag (modified from Li et al., 2021).

mudstone, argillaceous dolomite, dolomitic mudstone, sandstone, conglomerate, etc. In the early stage of P_1f_3, shallow lacustrine deposits were mainly argillaceous rocks (Xia et al., 2020). In the late depositional period, the terrigenous clastic sedimentary supply was higher. It deposited fine-grained siltstone, coarse-grained sandstone, and conglomerate (Li et al., 2021).

2.3.2. P_1f_2

The P_1f_2 is 150–600 m thick. It is mainly composed of mudstone, argillaceous sandstone, argillaceous dolomite, and dolomite, accompanied by a large number of alkaline minerals appearing (Cao et al., 2015). During this depositional period, the input of terrestrial clast was limited. It was a robust evaporative environment. The salinity and Ph of the lake were higher, which caused the deposition of a large amount of sodium carbonate and carbonate minerals (Xia et al., 2020).

2.3.3. P_1f_1

The thickness of P_1f_1 is 100–300 m. It is composed of terrigenous and volcanic clasts, including argillaceous dolomite and limestone, dolomite, tuffaceous rocks, and volcanic rocks. The lower part of P_1f_1 developed a large number of volcanic rocks (i.e., ignimbrite, andesite, and basalt), indicating that volcanic eruptions were frequent during this period (Yu et al., 2019). The upper part of P_1f_1 is organic-rich mudstone and dolomite, deposited during the expansion period of the lake (Li et al., 2021).

3. Samples and methods

3.1. Samples

One hundred eighty-eight samples from P_1f (P_1f_3, P_1f_2, and P_1f_1 collected 38, 123, and 27 samples, respectively.) were collected from nine wells (well depths between 3500 and 5000 m), i.e., MY1, AK1, FN1, FC1, FN2, FN3, FN14, FN409, and MH28 from the Mahu Sag to explore the source rock quality and shale oil resource potential. In particular, a large number of core samples were collected from the Well MY1. These cores are considered representative because they are collected in the most critical shale oil production well. Rock-Eval pyrolysis and total organic carbon (TOC) analysis were performed on 188 shale samples. In addition, some samples were selected for vitrinite reflectance Ro, maceral composition, X-ray diffraction (XRD), and scanning electron microscopy (SEM) analysis.

3.2. TOC and Rock-Eval pyrolysis

After surface cleaning, these samples were grounded into fine particles (200 mesh size) to analyze TOC and Rock-Eval pyrolysis. About 0.10 g of powdered sample was used for TOC analysis. Before analysis, samples were treated with diluted hydrochloric acid (5%) to remove carbonate minerals. Then the samples were washed with deionized water every half an hour, and the whole process lasted for three days. Later on, the samples were dried in an oven at 80 °C. The Leco CS-230 apparatus measured the residual organic carbon in the rock. Pyrolysis was carried out with Rock-Eval II instrument. At the beginning of pyrolysis, the oven was isothermally heated at 300 °C for 3 min, then the free hydrocarbon (S_1) was obtained. Then the oven temperature was increased to 600 °C at 25 °C/min, to determine the hydrocarbons generated from kerogen cracking (S_2).

3.3. Ro and maceral composition

The vitrinite reflectance (Ro) analysis was performed using an MPV-SP microscope using International Standard ISO 17246:2010. The sample was first embedded in liquid epoxy resin and then polished to a smooth surface after drying. Then the sample was immersed in oil and irradiated with monochromatic light. Before Ro measurement, the microscope was calibrated repeatedly. The measurement points were evenly distributed on the surface of the sample to ensure accuracy, and each sample was measured separately at least ten times. If the Ro standard deviation was greater than 0.05%, remeasure the sample. The determination of the maceral composition was carried out following ISO 7404 3:2009.

3.4. XRD

XRD analysis was performed using a D2 Phaser diffractometer. 5 g of the sample was taken and ground to 300 mesh and smeared on a glass slide for experimentation. After setting the experimental parameters of the device, perform measurement and analysis. Before separating the clay fraction, 15% acetic acid was used to remove the easily soluble carbonate and then continuously washed with deionized water. Stokes' law was applied to separate the clay fraction from the stabilized aqueous suspension. Then a paste was smeared on a glass slide to analyze the clay fraction after drying (Chen et al., 2018).

3.5. FE-SEM

Sigma 500 SEM was used to observe the microscopic pore structure of shale. The acceleration voltage of the experimental equipment was 20 keV, the magnification was up to 200,000 times, and the resolution is up to 0.8 nm. Before FE-SEM imaging, all samples were prepared with a specification of 10 × 5 × 1.5 mm (width, height, and length). Before the observation, the surface of the shale sample was coated with a 10 nm thickness of gold to increase the conductivity (Curtis et al., 2012b). Subsequently, an FE-SEM device was applied to observe the samples.

4. Results and discussion

4.1. Mineralogical composition

XRD analysis shows the P_1f shale is mainly dominated by quartz (averaging 29.74 wt%) and dolomite (averaging 25.09 wt%), followed by feldspar (averaging 18.29 wt%) and clay minerals (averaging 10.93 wt%) (Fig. 4A and B). Although dolomite is the main carbonate mineral, the calcite content is 8.97 wt%. Feldspar includes K-feldspar and plagioclase, having a concentration of 13.16 wt% and 5.13 wt%, respectively. A small amount of pyrite is also noticed in the studied samples averaging 4.57 wt%. The clay minerals mainly consist of the illite/smectite (I/S) mixed layer and illite, with average contents of 45.31 wt% and 42.12 wt%, respectively. The abundance of kaolinite and chlorite is low, with a mean of 3.92 wt% and 2.61 wt%, respectively. The three sub members of the P_1f have a similar mineral composition (Fig. 5A), and the quartz and dolomite are the main mineral content. The clay mineral content in P_1f_3 is higher than that of P_1f_2 and P_1f_1. There are obvious differences in the types of clay minerals in different sub-members (Fig. 5B). P_1f_1 has a significantly higher proportion of I/S mixed layer than P_1f_2 and P_1f_3, while kaolinite and chlorite are lower in P_1f_2 and P_1f_1.

The major North American shale reservoirs are abundant in brittle minerals (quartz, feldspar, and carbonate minerals). For instance, the Barnett Shale and Wolfcamp Shale have an average quartz content of 45% and 36%, respectively (Wilson et al., 2016). The calcite and dolomite content in Eagle Ford Shale is higher than 60% (Curtis et al., 2012a, 2012b). The content of brittle minerals in P_1f shale is higher than 60%, which is very beneficial for hydraulic fracking to increase permeability (Liu et al., 2019; Rybacki et al., 2016). Precious studies on unconventional shale oil and gas suggested the clay content in a favorable shale reservoir should be lower than 40% (Britt and Schoeffler, 2009; Rickman et al., 2008). The clay mineral content in P_1f shale is about 10%, indicating its potential to be a favorable shale oil reservoir.

The FE-SEM can be applied to observe the typical mineral features. Quartz exists in the intergranular pores or dissolution pores in different

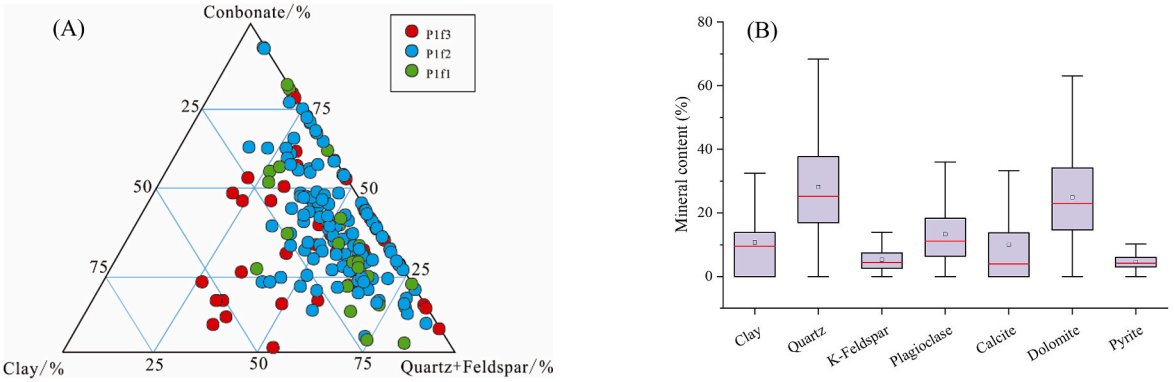

Fig. 4. Ternary diagram of the mineralogy (A) (after Liu et al., 2020) and distribution of mineral compositions (B) of the P_1f shale. The box provides the 25th and 75th percentiles, with the median value represented by the red line. The black square in the box indicates the mean value. (For interpretation of the references to colour in this figure legend, the reader is referred to the Web version of this article.)

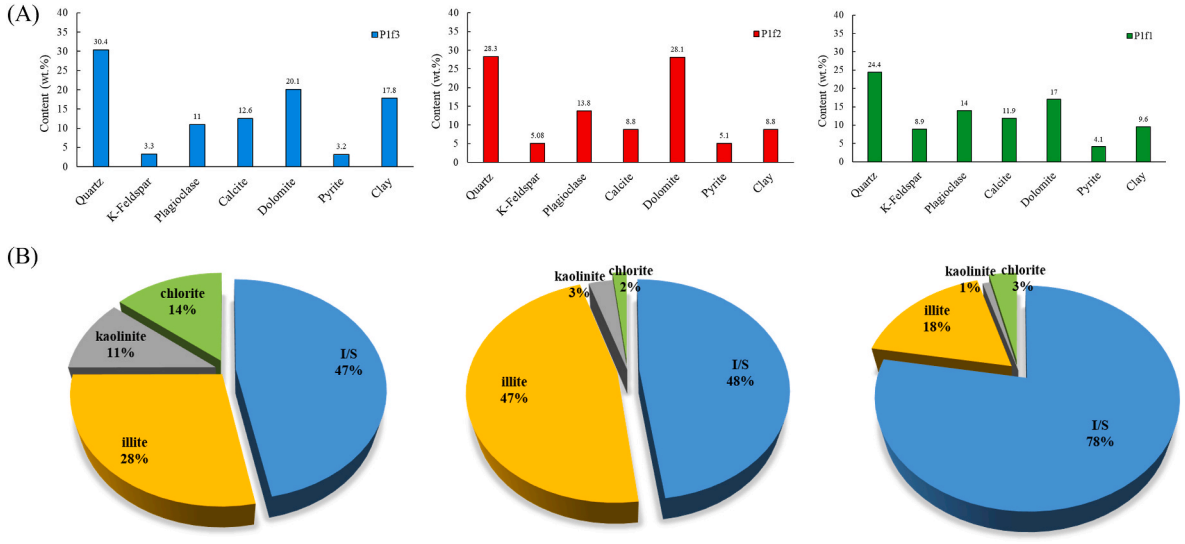

Fig. 5. Mineral composition (A) and clay fraction (B) characteristics of the P_1f shale.

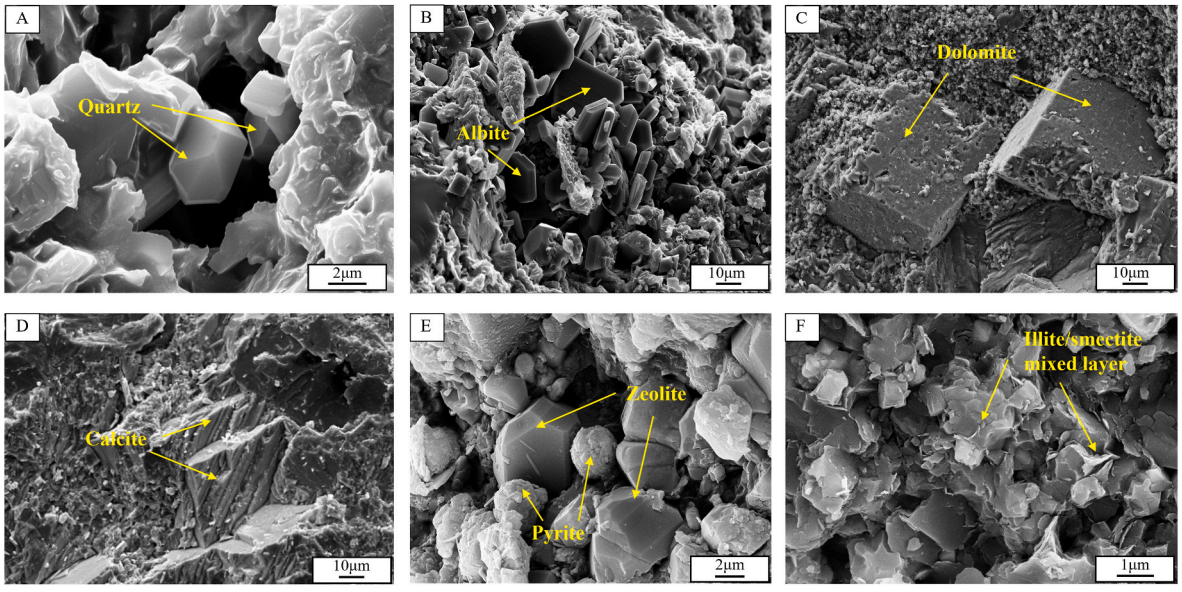

Fig. 6. Typical mineral characteristics of the P_1f shales. (a) Authigenic granular quartz crystal; (b) Tabular albite crystal; (c) Rhombohedral dolomite crystal; (d) Calcite crystal; (e) Granular pyrite and zeolite minerals; (f)Irregular I/S mixed layer.

forms (i.e., aggregates or individual granular), and the granular crystal form is well developed (Fig. 6A). Albite is more common among feldspars and appears in the form of plates, which can form good intercrystalline pores (Fig. 6B). The dolomite and calcite crystals are relatively developed and have regular shapes, often accompanied by partial dissolution (Fig. 6C and D). Pyrite often appears in agglomerates, accompanied by clay or zeolite minerals. It is mainly distributed in intergranular pores (Fig. 6E). The I/S mixed layer is widely developed, often in the form of slabs, skirt-like protrusions, and local honeycombs (Fig. 6F).

4.2. Geochemical characteristics

Evaluating the geochemical characteristics of organic matter (OM) can provide important guidance for assessing shale oil resource potential. Thus, this research first describes the geochemical characteristics of the P_1f shale.

4.2.1. Source rock generative potential

The OM is the material basis for hydrocarbon generation. TOC can be considered a direct measure of the OM abundance in source rocks (Hakimi et al., 2010; Hazra et al., 2017; Peters, 1986; Salama et al., 2021). The potential yield (PY) of shale is the sum of S_1 and S_2 values during the pyrolysis of the rock and is also called genetic potential (GP). It is also a good indicator to evaluate the OM abundance (Abd-Allah et al., 2019; Awan et al., 2020; Chen et al., 2018; Hakimi and Ahmed, 2016). S_1 (hydrocarbons formed before pyrolysis) is the volume of hydrocarbons produced by the source rock due to maturation. The residual hydrocarbon generation potential (S_2) is the hydrocarbons produced by the maturity increase during the burial process, and the value gradually decreases with the maturity increase. Table 1 shows the characteristic parameters of OM in source rocks of P_1f. The S_1 of shale varies from 0.5 to 4.0 mg HC/g Rock, averaging 1.25 mg HC/g Rock. The S_2 is between 0.5 and 8.0 mg HC/g Rock, with a mean value of 2.44 mg HC/g Rock. Higher GP values usually accompany good source rocks. In this research, it has been noticed the P_1f has a higher GP. The relationship between the S_2 and TOC shows the P_1f shale has a higher TOC and S_2 yield (Fig. 7A). This is consistent with the TOC vs. (S_1+S_2) plot, indicating the P_1f has good hydrocarbon generation potential (Fig. 7B). Moreover, the distribution of TOC and GP also reveals the P_1f shale has good OM abundance (Fig. 7C and D). The proportion of samples with TOC reaching good source rocks is more than 60%, and the GP shows the proportion of samples reaching medium-good source rocks is more than 50%. The abundance of OM in the three sub members of the P_1f is different (Table 1). The TOC and GP values of the P_1f_3 samples are 0.89 wt% and 4.25 mg HC/g Rock, respectively. The value of TOC in the P_1f_2 samples is 0.78 wt%, while the GP is 3.63 mg HC/g Rock. The TOC and GP of the P_1f_1 samples are 0.64 wt% and 3.99 mg HC/g Rock, respectively. Overall, the OM abundance in P_1f_3 and P_1f_2 is better than that of P_1f_1.

Additionally, the HI is also an important parameter reflecting the hydrocarbon generation ability (Hakimi et al., 2020). The results show the HI of the studied samples has a wide distribution, mainly ranging from 40 to 1280 mg HC/g TOC, with a mean of 310 mg HC/g TOC (Table 1). It should be noted that the currently measured HI is always lower than the original hydrocarbon generation potential (HI_o). The pyrolysis S_2 vs. TOC plot can be used to estimate the generative potential (Hakimi et al., 2010; Liu et al., 2019; Sanei et al., 2014). It indicates the P_1f shale mainly consists of oil-prone type II kerogen (Fig. 8). The regression lines show an obvious linear trend ($R^2 = 0.8019$) (Fig. 8). The slope of the straight line characterizes the trend-based HI_o, which is estimated to be 484 mg HC/g TOC (Slope × 100 = HI_o = 484 mg HC/g TOC), corresponding to the type II kerogen by previous researchers (Cornford et al., 1998).

4.2.2. Kerogen type and hydrocarbon generated

Different kerogens have different generative potentials, and the determination of the type of kerogen is very important for source rock evaluation (Hakimi and Ahmed, 2016; Makky et al., 2014). In this study, the kerogen type was identified by identifying pyrolysis parameters and maceral constituents. The cross plot between HI versus T_{max} and the Van Krevelen diagram (HI vs. OI) is used to classify and evaluate the kerogen type (Abdel-Fattah et al., 2017; Hakimi et al., 2010; Hakimi and Ahmed, 2016). According to the plotting of HI and T_{max}, the kerogen type in the studied samples is dominated by type II (Fig. 9A), consistent with the Van Krevelan diagram (Fig. 9B). The TOC and petroleum yield (S_2) diagram can also determine the kerogen type of the shale (Abd-Allah et al., 2019; Hakimi et al., 2020; Sanei et al., 2014), and the results show the studied shale is mainly of type II kerogen (Fig. 9C). In addition, the organic constituents can be used to classify the kerogen type (Hakimi and Ahmed, 2016). Table 2 shows the maceral composition of the studied samples. The source rock of the P_1f comprises various maceral groups, i.e., exinite, vitrinite, sapropelinite, and inertinite. The exinite maceral group ranges from 60.98% to 91.67% (averaging 75.87%), followed by the vitrinite, with an average value of 19.80%. The amount of sapropelinite and inertinite maceral groups is very low, averaging 3.08% and 1.26%, respectively. The ternary plot between various maceral groups of the three sub-members of the P_1f depicts the type of kerogen in the studied samples as mainly type II kerogen (Fig. 9D). Kerogen type index (TI = a+0.5 × b-0.75 × c-d, a: sapropelinite, b: exinite, c: vitrinite, d: inertinite) can also classify the type of kerogen (Li et al., 2019b). The TI of P_1f is lower than 40, with a mean value of 28.13, indicating type II kerogen. The results obtained by pyrolysis parameters are consistent with the results of maceral compositions.

4.2.3. Level of thermal maturity

Numerous thermal maturity indicators have been proposed (Heroux et al., 1979). The most used maturity indicators are vitrinite reflectance (R_o) and pyrolysis T_{max} (Abd-Allah et al., 2018; Hackley et al., 2015; Katz and Lin, 2021; Makky et al., 2014; Peters, 1986). Compared with the Ro value, T_{max} can be obtained quickly, and in large quantities, but the T_{max} value can easily be affected by other factors (i.e., kerogen type, asphaltene, and mineral composition.) (Dembicki et al., 1983; Katz and Lin, 2021; Peters, 1986; Peters et al., 2018). Therefore, vitrinite reflectance (R_o) is considered the best paraand 27 samples respectively. meter for studying the maturity and thermal evolution of kerogen (Abdel--Fattah et al., 2017; Hackley et al., 2015; Jin et al., 2021). The cross plot between R_o and the burial depth of the studied well shows the association between burial depth and maturity in the study area (Fig. 10A). It shows with an increase in depth, the thermal maturity also increases. According to Fig. 10, the source rock enters the oil window at a depth of

Table 1
Geochemical characteristics of the P_1f shale.

Sub-member	TOC (wt.%)	S_1 (mg HC/g Rock)	S_2 (mg HC/g Rock)	T_{max} (°C)	GP (mg HC/g Rock)	HI
P_1f_3	0.14–2.95 (0.89)	0.14–4.26 (1.23)	0.08–19.90 (3.015)	409-458 (429)	(0.23–20.81) 4.25	(50–702) 270
P_1f_2	0.08–2.06 (0.78)	0.02–3.50 (1.09)	0.05–12.43 (2.54)	401-448 (431)	0.07–13.0 (3.63)	(50–1280) 326
P_1f_1	0.08–2.31 (0.64)	0.01–8.39 (1.77)	0.03–14.69 (2.21)	401-448 (419)	0.10–15.08 (3.99)	(40–636) 255

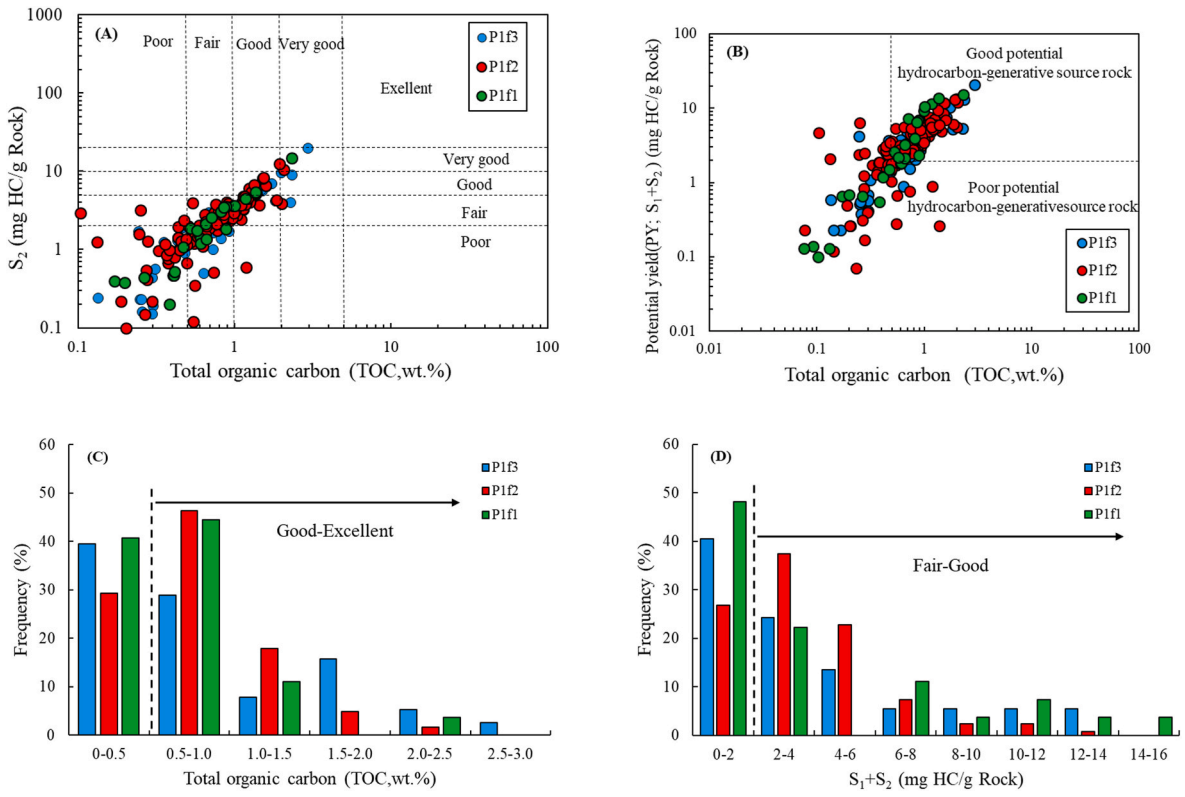

Fig. 7. Geochemical characteristics of the P_1f shales. (A) Plot of TOC vs. S_2 (after Hakimi et al., 2016), (B) TOC vs. GP (after Hakimi et al., 2016) for the analyzed source-rock samples. (C) Frequency diagrams of TOC and (D) GP of shale samples.

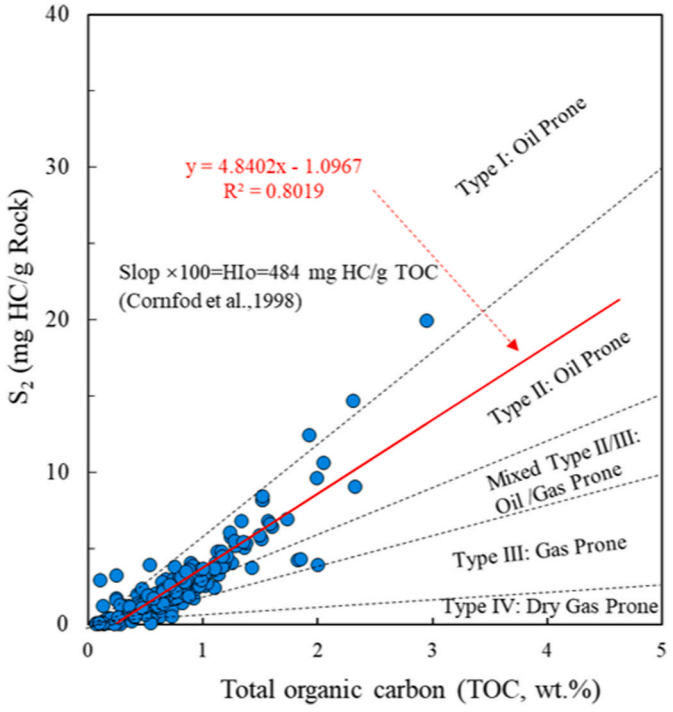

Fig. 8. Relationship between TOC content and S_2 yield (after Sanei et al., 2014).

3000 m. It also reveals the source rock of the P_1f is thermally mature to high-mature. Similarly, there is also a positive association between T_{max} and burial depth (Fig. 10B). However, the T_{max} value of the studied samples is mainly distributed between 420 °C–440 °C, indicating the source rock is immature to early mature. Feng et al. (2020) and Tang et al. (2021) used biomarker compounds to study the thermal maturity of the P_1f, suggesting the source rocks have reached the mature stage. Moreover, the abnormal T_{max} may be related to the residual asphaltenes in the shale.

Additionally, basin modeling is used for studying the burial history and thermal evolution history of P_1f shale. The measured Ro is used to constrain and correct the thermal evolution history. The burial history in the north of the sag shows the characteristics of rapid deep burial in the early period and slower burial in the late period based on PetroMod simulation results (Fig. 11). Due to the rapid burial of the strata and the high heat flow, the Ro of the source rock reached 0.50% in the late Permian. In the Late Triassic, the degree of thermal evolution was higher (Ro>0.80%). After that, the Mahu sag only experienced uplift and denudation in the late Jurassic. The entire burial depth has increased gradually, as has thermal maturity. At present, the source rock has reached a mature to high-mature stage. It should be noted that the current wells are only distributed on the edge of the Mahu Sag. In these areas, the P_1f has a shallow burial depth (<5000 m), and the source rock with a greater burial depth (>6000 m) has a higher R_o inside the sag is presumed to exist abundant gaseous hydrocarbons (Tao et al., 2019).

4.3. Reservoir quality

Shale oil is hydrocarbons that have not been expelled and remained in-situ. Therefore, reservoir quality is a crucial factor affecting shale oil potential (Li et al., 2021; Loucks et al., 2012). Shale is characterized by poor petrophysical properties and extremely small storage space (Clarkson et al., 2012; Huang et al., 2020a; Loucks et al., 2012). And pores and fractures play a significant role in shale reservoirs. They provide effective storage space and remarkably improve fluid flow capacity (Liu et al., 2020; Wang et al., 2015). In addition, conventional shale oil production technology is difficult to obtain industrial production capacity. Therefore, fracturing technology must be utilized, which

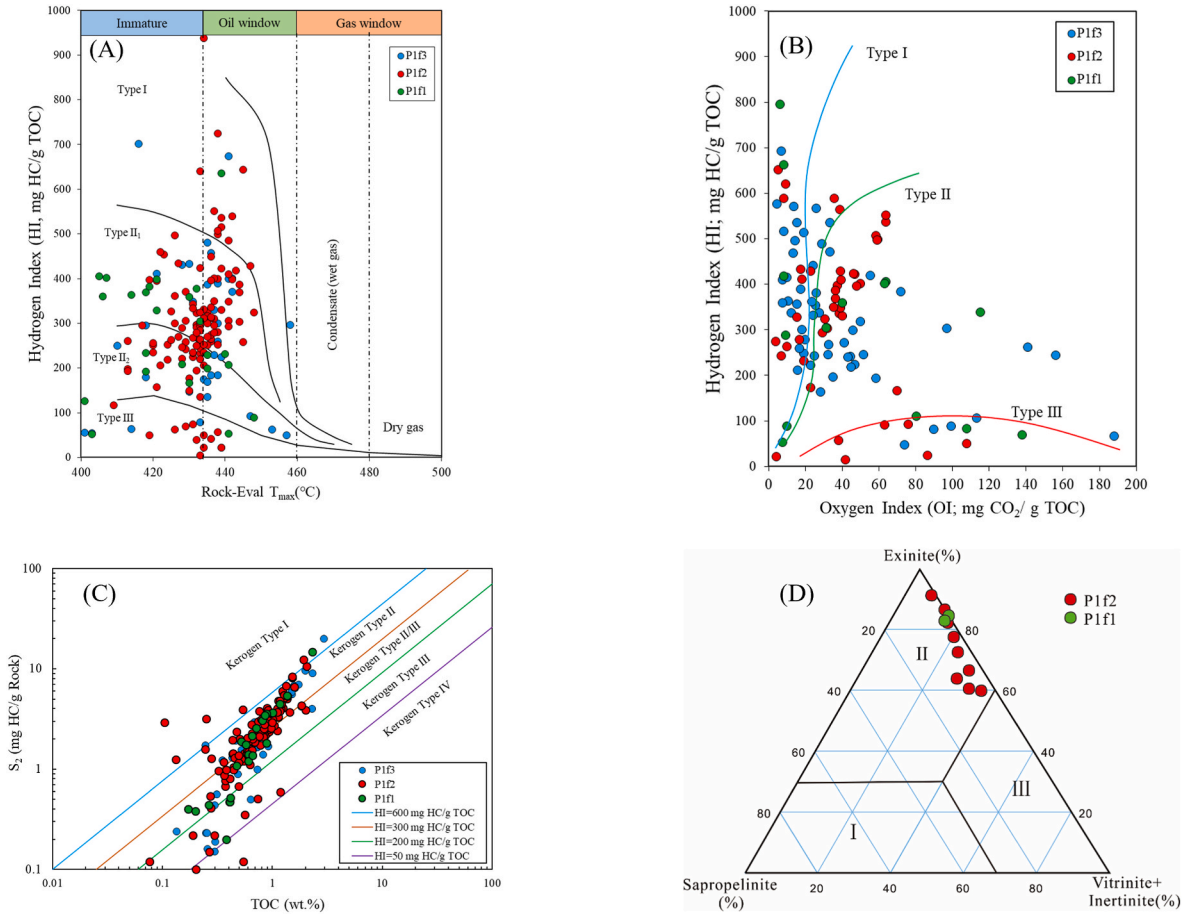

Fig. 9. Diagram showing the kerogen type. (A) HI vs. T_{max} (after Peters, 1986); (B) HI vs. OI (after Peters, 1986; Makky et al., 2014); (C) Plot of TOC and S_2 (after Hakimi et al., 2020); (D) The ternary diagram of maceral composition (after Wang et al., 2015).

Table 2
Maceral composition of the analyzed samples.

Sample	Sub-member	Lithology	Macerals analysis (%)				TI	Kerogen type
			Sapropelinite	Exinite	Vitrinite	Inertinite		
M-1	P_1f_2	Dolomitic mudstone	2.30	78.16	17.82	1.72	32.16	II_2
M-2	P_1f_2	Mudstone	4.03	60.48	33.06	2.42	15.63	II_2
M-3	P_1f_2	Calcareous mudstone	3.73	67.08	27.95	1.24	19.81	II_2
M-4	P_1f_2	Dolomitic mudstone	8.47	64.41	25.85	1.27	22.90	II_2
M-5	P_1f_2	Mudstone	/	87.13	11.03	1.84	34.39	II_2
M-6	P_1f_2	Mudstone	1.42	82.94	14.69	0.95	34.15	II_2
M-7	P_1f_2	Dolomitic mudstone	3.85	73.08	22.12	0.96	26.92	II_2
M-8	P_1f_2	Dolomitic mudstone	6.91	60.98	31.30	0.81	14.49	II_2
M-9	P_1f_2	Dolomitic mudstone	1.28	91.67	7.05	/	42.92	II_1
M-10	P_1f_1	Dolomitic mudstone	/	85.12	13.02	1.86	31.72	II_2
M-11	P_1f_1	Mudstone	1.87	83.52	13.86	0.75	34.40	II_2
Average values			3.76	75.87	19.80	1.38	28.14	/

is critical to shale oil's successful exploitation (Curtis, 2002; Zhou et al., 2021). Thus, the fracability of the reservoir is also a key parameter for evaluating the shale oil potential.

4.3.1. Pores and fractures

Previous research mainly focuses on the role of its source rock quality, and less attention has been paid to its ability as an oil and gas reservoir. Thus, there are few studies on the reservoir characterization of the P_1f (Li et al., 2021; Yu et al., 2018a; Zhi et al., 2021). In our study, the fractures and pores in the P_1f were systematically evaluated from two different perspectives (macroscopic and microscopic), using core scanning images and FE-SEM. The core scanning images show that there are microfractures and macrofractures in the shale of the P_1f. Among them, microfractures are often smaller in size, having lengths of centimeters or less and widths of millimeters. They often cause partial laminar dislocation, and part of the microfractures have been filled by carbonate minerals (Fig. 11). By comparison, the microfractures are large scale and usually extend at an angle of nearly 90°, with vertical lengths of meters or more, but are less developed. There are excellent fluid transport channels due to being partially filled or unfilled. Although the filled fractures cannot be directly used as seepage channels, they can still be favorable targets for hydraulic fracturing due to the fragility of the water-rock interface (Walton and McLe, 2013; Wang et al., 2015). Fluorescence scanning of the core shows the control effect

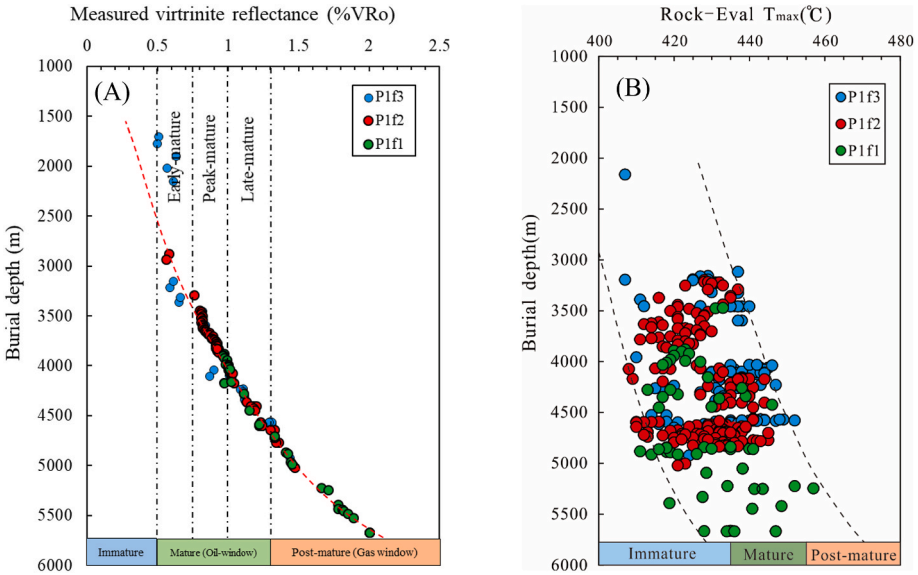

Fig. 10. Plots of Ro and T_{max} vs. burial depth of the P_1f in the Mahu Sag.

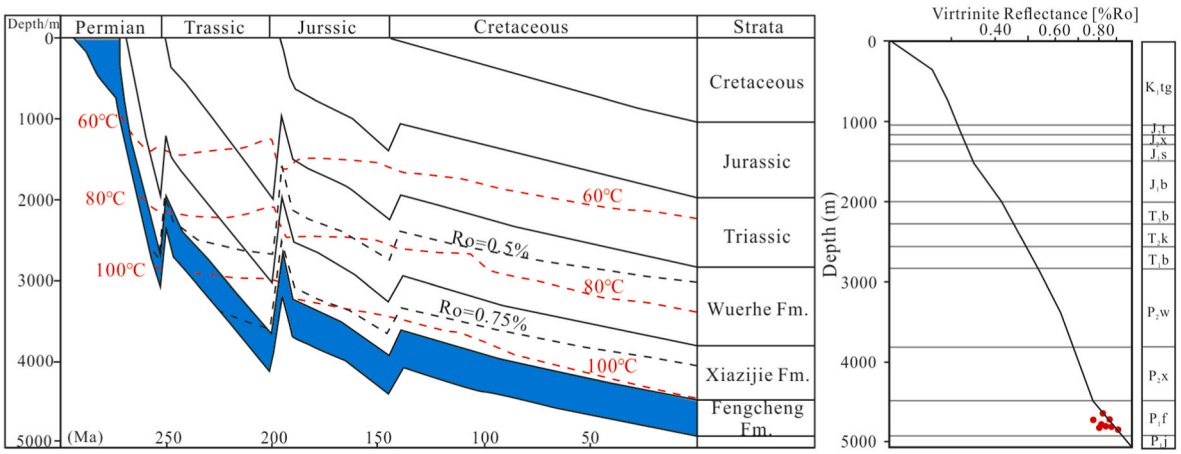

Fig. 11. Burial and thermal evolution histories of Well MY1 in the Mahu Sag.

of pores and fractures on hydrocarbons. The density of the fractures observed by fluorescence scanning is about (3–5) fractures/10 cm, a width usually less than 2 mm and a small length, existing concentrated development sections of fractures (Fig. 12).

Previous studies have shown various types of developed pores in shales (Clarkson et al., 2012; Curtis et al., 2012b; Huang et al., 2020b; Liu et al., 2020; Loucks et al., 2012). However, the pores of alkaline lacustrine shale, including the P_1f shale, have not been thoroughly studied. In this study, various nano-micron pores are observed in shale using FE-SEM. Mineral matrix pores mainly dominate these pores. Intergranular pores are mainly developed between brittle minerals. They are generally irregular pores with a width of several hundred nanometers (Fig. 13a). In some samples, intergranular micropores are also developed in the clay minerals, mainly in curved sheets and irregular shapes, with a size between 0.1–10 μm (Fig. 13b, c). Intragranular pores are mostly found in dissolved feldspar particles (Fig. 13g), carbonate minerals (Fig. 13e), and siliceous minerals (Fig. 13f). Most of them have irregular closed contours, with a pore size between 0.05–20 μm. The degree of organic pore development is affected by kerogen type and thermal maturity (Curtis et al., 2012a; Ko et al., 2016). The organic pores in the study area are bubble-like, with widths varying from tens to hundreds of nanometers (Fig. 13h). The connected and effective pore network did not develop in organic pores compared to intragranular pores and intergranular pores. Additionally, microfractures formed by squeezing rigid particles have been observed in the studied samples (Fig. 13i), which often serve as high-permeability pathways for fluids flow.

4.3.2. Physical properties

The petrophysical properties of organic-rich shale are crucial for evaluating commercial quantities of unconventional hydrocarbons (Liu et al., 2019). The multi-source mixed sediments of the alkaline lacustrine condition of the P_1f formed multiple types of reservoir rock. This research only discusses the shale and calcareous/dolomitic shale. However, the sandstone and volcanic rocks that are outside the scope of discussion. The statistics of the physical properties are shown in Fig. 14A and B. The porosity of the P_1f is between 1.0% and 12.0%, averaging 3.37%. Moreover, the samples comprising porosity greater than 6% are about 16.47%. The average permeability is about 0.024 mD and samples smaller than $0.1 \times 10^3 \mu m^2$ account for 80%. Generally, the physical properties of P_1f_1 and P_1f_2 are better than P_1f_3.

Brittleness is a key parameter that has a great impact on shale fracability (Curtis, 2002). The mineral composition of the rock affects its brittleness. Rock with more brittle minerals have better engineering fracturing effects (Curtis, 2002; Rickman et al., 2008). At present, the brittleness index (BI) and rock mechanical parameters (i.e., Young's

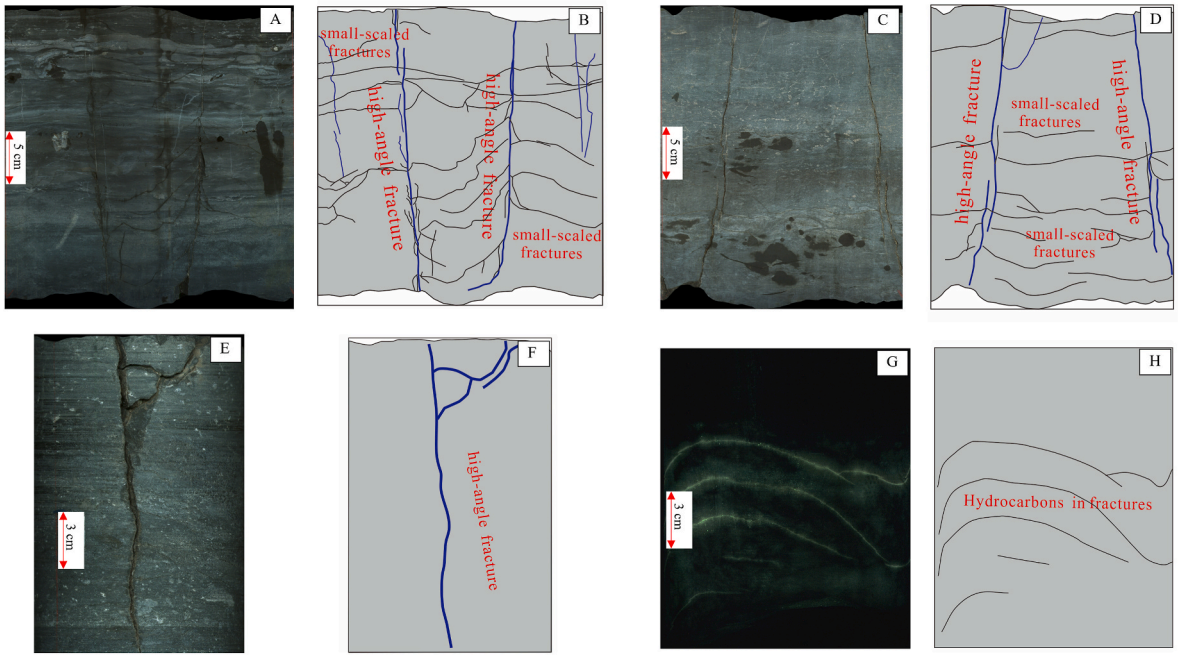

Fig. 12. Characteristics of fractures from the core images in the P_1f shale.

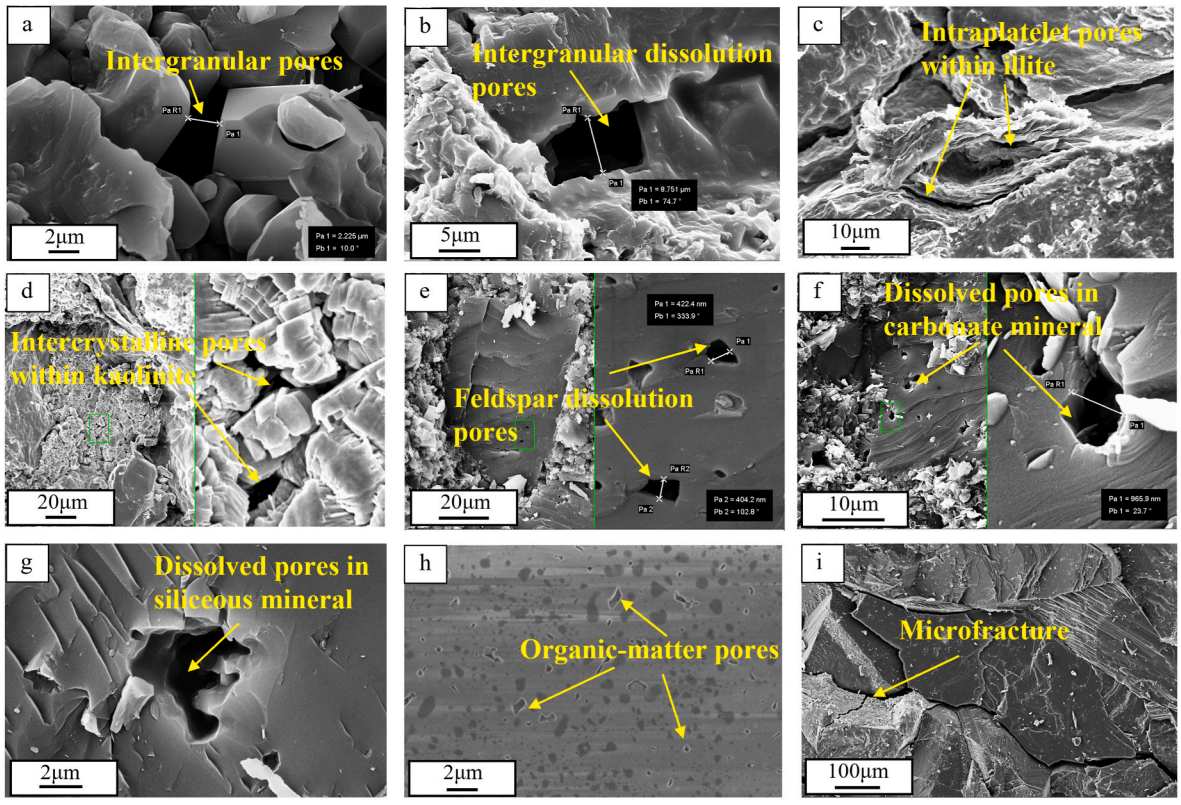

Fig. 13. The representative pore types in the shale. (a) Intergranular pores between the quartz grains; (b) Intergranular dissolution pore; (c) Intercrystalline pores within illite; (d) Intercrystalline pores within kaolinite; (e) Dissolved pores in feldspar grains; (f) Dissolved pores in carbonate mineral grains; (g) Dissolved pores in siliceous mineral grains; (h) Organic pores; (i) Microfractures.

modulus, Poisson's ratio) are widely used to evaluate the fracturing ability of the formation (Awan et al., 2021; Gholami et al., 2016; Jiang et al., 2010; Rickman et al., 2008). Studies have shown that the higher the content of brittle minerals in the rock, the greater its Young's modulus and the lower its Poisson's ratio (Gholami et al., 2016; Rickman et al., 2008). In this study, we comprehensively considered these parameters to evaluate the brittleness of the P_1f shale. Previous research used mineral composition to calculate the BI formula as follows (Zhang et al., 2021a; Zhou et al., 2021):

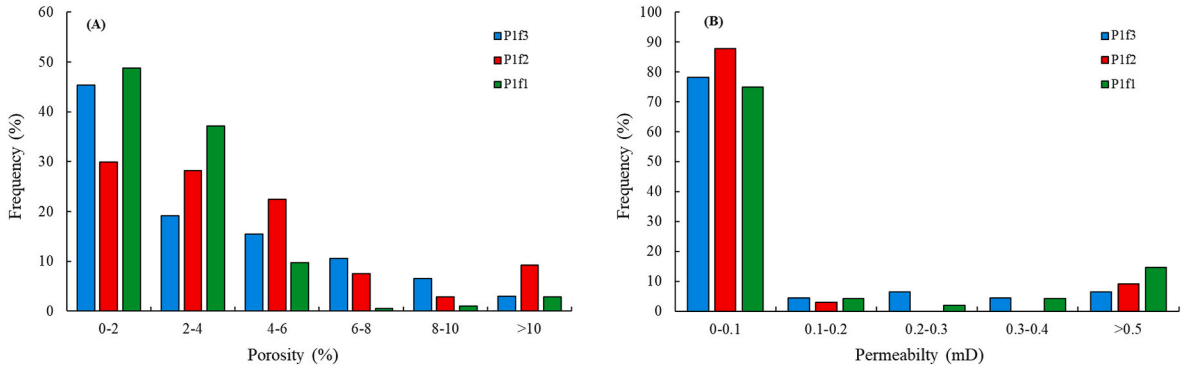

Fig. 14. Porosity and permeability are characteristic of the shale.

$$BI = (Q_Z + Car + Fels) / (Q_Z + Car + Fels + Clay) \times 100\%$$

In the formula, Q_Z, *Car*, *Fels*, and *Clay* represent the content of quartz, carbonate, feldspar, and clay minerals. The BI of the P_1f shale is generally between 80% and 90%, with an average of 84%. There are slight differences in different sub members. Among them, P_1f_1 has the highest BI (with a mean value of 85.74%), followed by P_1f_2 (averaging 84.86%), while the BI of P_1f_3 is relatively lower (with an average of 78.58%) (Fig. 15A). The BI of Barnett Shale is 46.4% (Zhou et al., 2021). It indicates the shale of the P_1f has excellent brittle nature. Jiang et al. (2010) suggested when Young's modulus is > 20 GPa, and the Poisson's ratio is < 0.25, the reservoir is more favorable for hydraulic fracturing. The Young's modulus of the P_1f in the study area is greater than 40 GPa, and the Poisson's ratio is between 0.23 and 0.3 (Fig. 15B). Based on the evaluation of the brittleness of the P_1f, compared with global commercial unconventional shale, it is suggested the P_1f shale has favorable conditions of petrophysical properties, indicating the shale has a strong fracture-making ability and good fracability.

4.4. Shale oil potential

The quantitative evaluation of resource potential is of great significance to shale oil exploration and exploitation (Chen et al., 2017; Li et al., 2019; Lu et al., 2012). Although the research on shale oil has made great progress in recent years, many factors affect the shale oil potential (including source rock quality, reservoir properties, oil content, etc.) (He et al., 2016; Hu et al., 2021b; Jarvie, 2014; Li et al., 2016). Thus, the potential of shale oil has not been well constrained. Of these many factors, the oil content is the most critical controlling factor.

4.4.1. Oil content evaluation and shale oil potential

Quantitative evaluation of oil content is vital for assessing shale oil potential (Chen et al., 2017; Hu et al., 2018; Li et al., 2019; Lu et al., 2012). The oil content of shale varies greatly, which is affected by the combination of mineral composition, OM characteristics, generative potential, and expulsion efficiency (Hu et al., 2021a; Li et al., 2016). The plot between S_1 and TOC can be used to distinguish between indigenous and migrated hydrocarbons (Jin et al., 2012; Salama et al., 2021; Sonnenberg et al., 2011). The plot of S_1 TOC of the P_1f shale is shown in Fig. 16A, revealing some samples with migrating hydrocarbons and high oil saturation, indicating the shale has good oil-bearing properties. The performance of the three sub members of the P_1f on the plot is similar, revealing the P_1f shale has good exploration and exploitation potential.

Lu et al. (2012) divided shale oil resources into three levels: enriched, potential, and ineffective resources. This classification method is widely used and has become a good indicator for the evaluation of shale oil resources (Chen et al., 2017; Hu et al., 2018). Fig. 16B shows the classification results of the P_1f shale: ①The enriched resource with the greatest oil potential (S_1 > 2.0 mg/g); ②The potential resource, the shale oil content (2 mg/g) g > S_1 > 0.5 mg/g); ③Ineffective resources, the relative oil content of the sample is low (S_1 < 0.5 mg/g). It can be seen that enriched resources and potential resources are the most important resource types (Fig. 15B), indicating the shale of P_1f has good shale oil exploration potential. Nevertheless, this methodology does not consider the production capacity of shale reservoirs and shale oil recovery. Jarvie (2012) suggested that evaluating the mobility of hydrocarbons in shale is more important and proposed the oil saturation index (OSI) to determine the oil production potential of a formation quickly. Many studies and exploration practices have shown that OSI is a practical indicator for estimating the potential of shale reservoirs. When OSI >100 mg/g, shale formations often have higher oil production. Through statistical analysis of the OSI data of the P_1f shale (Fig. 15B), the OSI in the studied area far exceeds 100 mg/g, with an average value of 181.95 mg/g. From the perspective of different sub members, the OSI of P_1f_1 is relatively low, with a mean of 124.21 mg/g, while P_1f_2 (OSI = 172.30 mg/g) and P_1f_3 (OSI = 161.13 mg/g) have the high OSI, indicating the most favorable shale oil-producing strata.

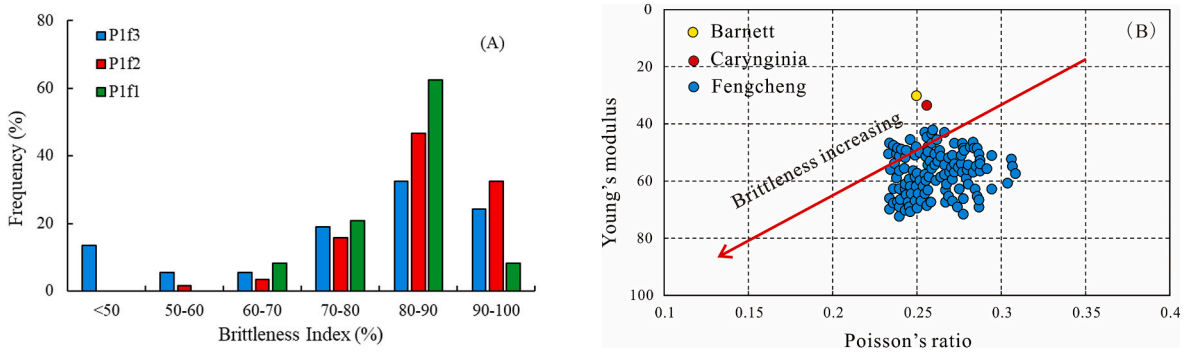

Fig. 15. Physical properties of the P_1f shale. (A) Distribution frequency of BI values; (B) Crossplot of Poisson's ratio and Young's modulus.

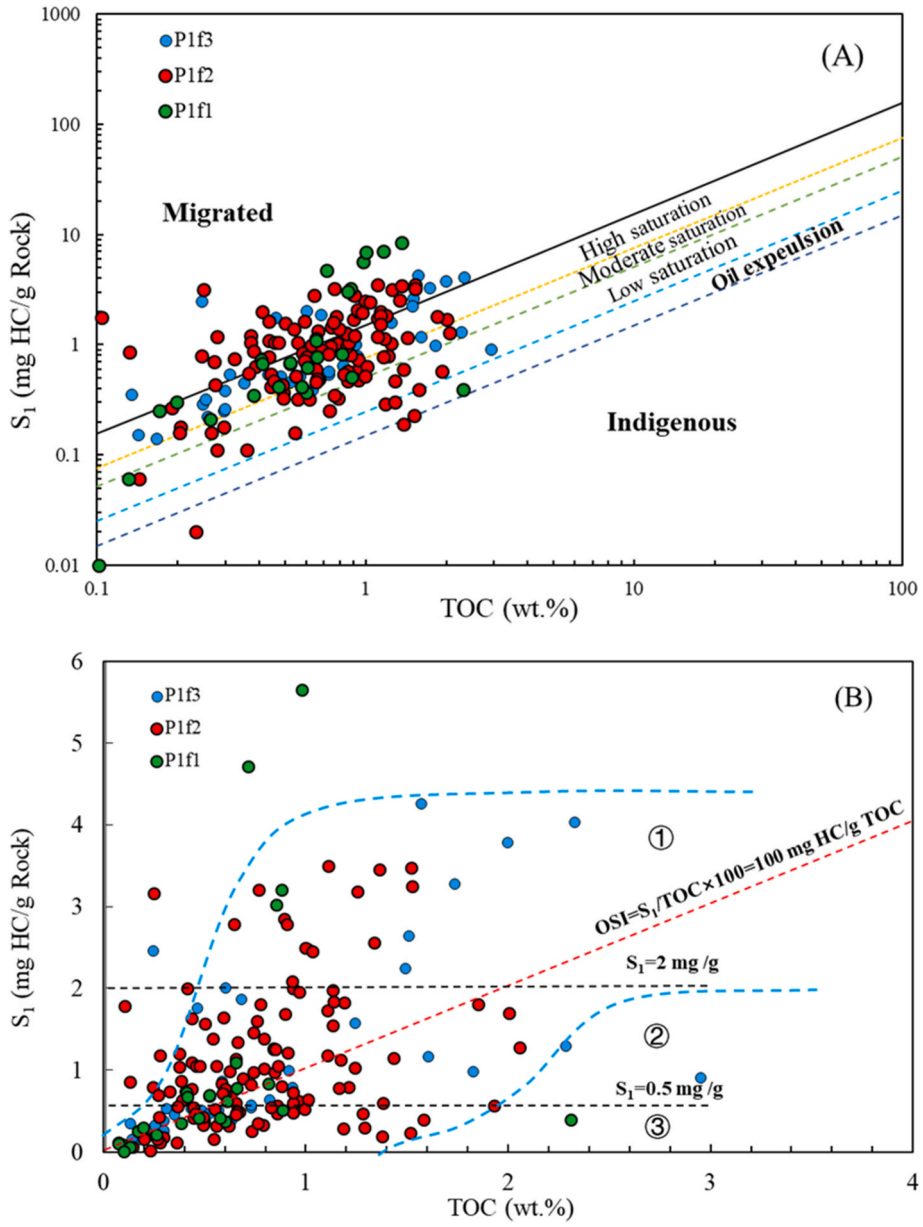

Fig. 16. Cross-plot of TOC vs. S_1 suggesting a part of migrated hydrocarbon (A) (after Jin et al., 2012) and showing the determination of the evaluation threshold of shale oil (B) (modified after Lu et al., 2012).

4.4.2. Comparisons with other crucial shales in the world

In the context of the above analysis, this research compares the characteristics of P_1f shale with the global commercial shale formations (Fig. 17). The major North American shales are mainly marine shales. Moreover, these global reservoirs have good continuity and are composed of variegated lithology (e.g., the combination of organic-rich shale, clastic rocks, and carbonate rocks). The marine shales are dominated by type I and type II_1 kerogen, and the OM abundance is generally high (usually TOC> 2%) (Curtis et al., 2012b; Ko et al., 2018; Loucks et al., 2012; Marra, 2018; Zhang et al., 2021b). For example, the Bakken Shale serves as a source and reservoir to a world-class shale oil accumulation in the Williston Basin. The formation consists of shale, dolomite, and limestone alternately, and the thickness of the shale is about 20–50 m. The maturity (Ro) is between 0.7% and 1.3%, and the TOC ranges from 10.0 wt% to 3.0 wt%, mainly type I and II_1 kerogen. The thickness of the lacustrine shale of the P_1f (200–300 m) in the Mahu Sag is much higher than the shales in North America, consistent with the shale of the Qingshankou Shale in the Songliao Basin (Fig. 17A). However, the shale of the P_1f is much deeper than other typical shales around the globe, and it is in the field of deep petroleum exploration. Additionally, compared with typical shale in other basins in North America and China, the TOC content of P_1f shale is lower, with an average value of less than 1.0 wt% (Fig. 17B). Generally, the shale in favorable shale oil-producing zones usually has a TOC >2.0 wt%. However, Zou et al. (2012) suggested that when the TOC is less than 2.0 wt%, shale with a thickness of more than 50 m can also be a commercially developed shale oil-producing zone. The OM abundance affects hydrocarbon generation and has a significant impact on hydrocarbon retention. Normally, the adsorbed hydrocarbons in shale are mainly adsorbed by OM (Chen et al., 2018; Hu et al., 2021a). It indicates the OM in the P_1f shale has a relatively weak adsorption capacity for hydrocarbons. Meanwhile, the maturity of the North American shale is generally high. For example, the Woodford Shale, the Eagle Ford Shale, and the Barnett Shale have Ro greater than 1.0%. The Ro of the P_1f shale is between 0.8% and 2.0%, reaching a medium to high maturity stage, and can produce abundant petroleum. In addition, the petrophysical

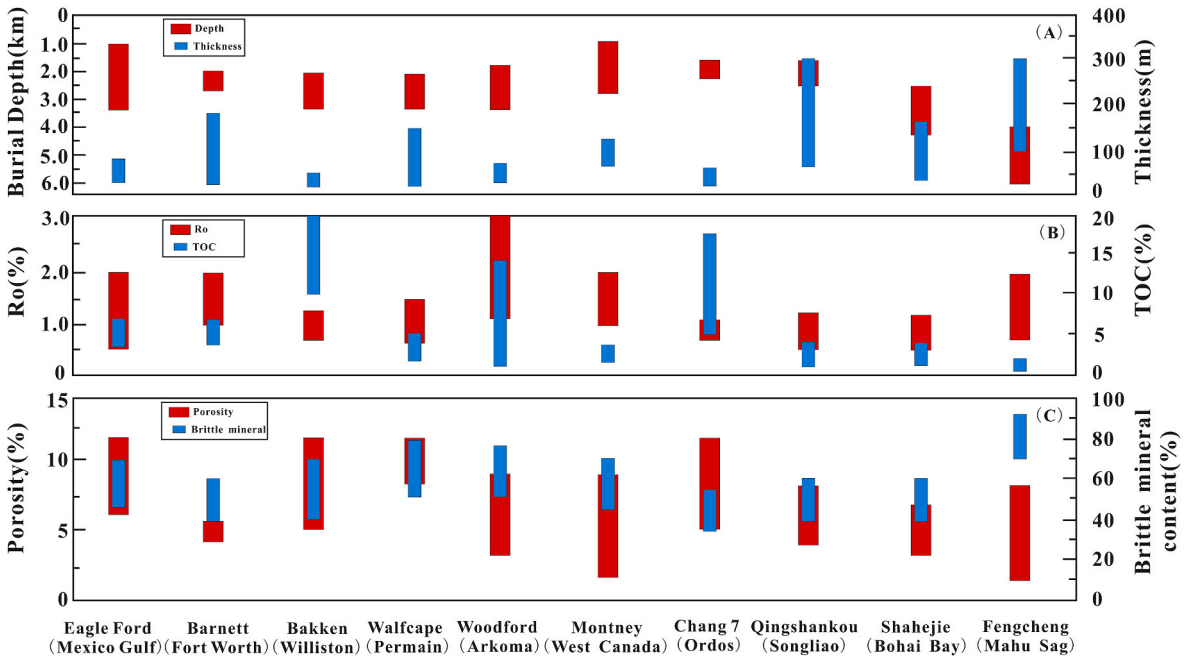

Fig. 17. General properties of major shale oil systems around the world (primary data are from Curtis et al., 2012; Loucks et al., 2012; Zou et al., 2014; Ko et al., 2018; Marra, 2018; Zhao et al., 2020; Zhang et al., 2021b). (A) Burial depth and thickness of major shale oil systems worldwide and the Mahu Sag. (B) Ro and TOC of major shale oil systems worldwide and the Mahu Sag. (C) Porosity and brittleness mineral content of major shale oil systems worldwide and the Mahu Sag.

properties of the P_1f are different from shale in other regions. The shale has poor porosity (Fig. 17C), but microfractures are well developed. It is related to the high abundance of brittle minerals (>70%) in shale (Fig. 17C). The mineral composition of shale affects the brittleness of the rock. Consequently, it affects the fracturing of the shale (Awan et al., 2021; Chen et al., 2018; Curtis, 2002; Rybacki et al., 2016). Thus, the unique petrophysical properties of the P_1f shale determine that it has good exploitation potential.

5. Conclusions

(1) Geochemical analysis of the P_1f shale in the Mahu Sag shows the shale has moderate TOC (averaging 0.80%), and high PG (averaging 3.95 mg HC/g TOC), and mainly types II oil-prone kerogen. The vitrinite reflectance R_o reveals the source rock is currently in a mature to the high-mature stage. Shale's original hydrocarbon generation potential can be as high as 484 mg HC/g Rock, which has good generative potential. The quality of the shale in the middle part (P_1f_2) is the best.

(2) P_1f shale has a higher concentration of brittle minerals, rich in calcite and dolomite, averaging 25.09 wt% and 8.97 wt%, respectively. However, the clay content is lower (10.93 wt%). Different types of pores have developed in the P_1f shale, mainly inorganic pores. Fractures are extremely developed, including microfractures and macrofractures. Although the shale has poor porosity and permeability, its brittleness index is higher than marine shale. It has good petrophysical properties for hydraulic fracturing.

(3) The plot of S_1 versus TOC shows a lot of retained hydrocarbons in the shale of P_1f, and the OSI is much greater than 100 mg HC/g TOC, suggesting the shale has a high content of movable oil. Comparing the geochemical indicators and reservoir characteristics of the P_1f shale with other global shales shows the P_1f shale is characterized by high thickness, high maturity, good oil content, and ease of fracturing. Thus, it is a favorable target for shale oil exploration and exploitation.

Author contributions

All authors discussed the results and contributed to the final manuscript.

Yuping Wu: Conceptualization, Methodology, Data curation, Formal analysis, Writing-Original Draft, Writing - Review & Editing.

Chenglin Liu: Supervision, Funding acquisition, Project administration, Visualization.

Fujie Jiang: Funding acquisition, Project administration.

Tao Hu: Conceptualization, Validation, Writing-Review & Editing.

Jiahao Lv: Data curation, Investigation.

Chenxi Zhang: Data curation, Investigation.

Xuguang Guo: Resources, Data curation.

Liliang Huang: Resources, Data curation.

Meiling Hu: Investigation.

Renda Huang: Investigation.

Rizwan Sarwar: Writing-Original Draft.

Yi Zhao: Resources.

Declaration of competing interest

The authors declare that they have no known competing financial interests or personal relationships that could have appeared to influence the work reported in this paper.

Acknowledgments

This research is financially funded by the National Natural Science Foundation of China of China (41872127, 41872128), the Strategic Cooperation Technology Projects of CNPC and CUPB (ZLZX2020-01-05), Science Foundation of China University of Petroleum (Beijing) (2462019BJRC005), and Young Talents Support Project of Beijing Science and Technology Association (ZX20210075).

References

Abd-Allah, Z.M., Abdullah, W.H., Abdel-Fattah, M.I., 2019. Assessment of eocene, paleocene and cretaceous source rocks in the west feiran area, offshore gulf of suez, Egypt. J. Petrol. Sci. Eng. 180, 756–772.

Abd-Allah, Z.M., Maky, A.F., Ramadan, M.A.M., 2018. Organic source of crude oils and 1d basin modeling of upper cretaceous rocks, badr concession, abu gharadig basin, western desert, Egypt. Arabian J. Geosci. 11, 13.

Abdel-Fattah, M.I., Pigott, J.D., Abd-Allah, Z.M., 2017. Integrative 1D-2d basin modeling of the cretaceous beni suef basin, western desert, Egypt. J. Petrol. Sci. Eng. 153, 297–313.

Awan, R.S., Liu, C., Aadil, N., Yasin, Q., Salaam, A., Hussain, A., Yang, S., Jadoon, A.K., Wu, Y., Gul, M.A., 2021. Organic geochemical evaluation of cretaceous talhar shale for shale oil and gas potential from lower indus basin, Pakistan. J. Petrol. Sci. Eng. 200.

Awan, R.S., Liu, C., Gong, H., Dun, C., Tong, C., Chamssidini, L.G., 2020. Paleo-sedimentary environment in relation to enrichment of organic matter of Early Cambrian black rocks of Niutitang Formation from Xiangxi area China. Mar. Petrol. Geol. 112.

Britt, L.K., Schoeffler, J., 2009. The Geomechanics of A Shale Play: what Makes A Shale Prospective. SPE Eastern Regional Meeting.

Cao, J., Lei, D., Li, Y., Tang, Y., Wang, T., 2015. Ancient high-quality alkaline lacustrine source rocks discovered in the lower permian Fengcheng Formation, Junggar Basin. Acta Pet. Sin. 36, 781–790.

Cao, J., Xia, L., Wang, T., Zhi, D., Tang, Y., Li, W., 2020. An alkaline lake in the Late Paleozoic Ice Age (LPIA): a review and new insights into paleoenvironment and petroleum geology. Earth Sci. Rev. 202.

Chen, G., Lu, S., Zhang, J., Wang, M., Li, J., Xu, C., Pervukhina, M., Wang, J., 2017. Estimation of enriched shale oil resource potential in E2s4L of damintun sag in bohai Bay basin, China. Energy Fuels 31, 3635–3642.

Chen, Z., Jiang, W., Zhang, L., Zha, M., 2018. Organic matter, mineral composition, pore size, and gas sorption capacity of lacustrine mudstones: implications for the shale oil and gas exploration in the Dongying depression, eastern China. AAPG (Am. Assoc. Pet. Geol.) Bull. 102, 1565–1600.

Clarkson, C.R., Freeman, M., He, L., Agamalian, M., Melnichenko, Y.B., Mastalerz, M., Bustin, R.M., Radliński, A.P., Blach, T.P., 2012. Characterization of tight gas reservoir pore structure using USANS/SANS and gas adsorption analysis. Fuel 95, 371–385.

Cornford, C., Gardner, P., Burgess, C., 1998. Geochemical truths in large data sets. I: geochemical screening data. Org. Geochem. 29, 519–530.

Curtis, J.B., 2002. Fractured shale-gas systems. AAPG (Am. Assoc. Pet. Geol.) Bull. 86 (11), 1921–1938.

Curtis, M.E., Cardott, B.J., Sondergeld, C.H., Rai, C.S., 2012a. Development of organic porosity in the Woodford Shale with increasing thermal maturity. Int. J. Coal Geol. 103, 26–31.

Curtis, M.E., Sondergeld, C.H., Ambrose, R.J., Rai, C.S., 2012b. Microstructural investigation of gas shales in two and three dimensions using nanometer-scale resolution imaging. AAPG (Am. Assoc. Pet. Geol.) Bull. 96, 665–677.

Dembicki, H., Horsfield, B., Ho, T., 1983. Source rock evaluation by pyrolysis-gas chromatography. AAPG (Am. Assoc. Pet. Geol.) Bull. 67.

Feng, C., Li, T., He, W., Zheng, M., 2020. Organic geochemical traits and paleo-depositional conditions of source rocks from the Carboniferous to Permian sediments of the northern Mahu Sag, Junggar Basin, China. J. Petrol. Sci. Eng. 191.

Gholami, R., Rasouli, V., Sarmadivaleh, M., Minaeian, V., Fakhari, N., 2016. Brittleness of gas shale reservoirs: a case study from the north Perth basin, Australia. J. Nat. Gas Sci. Eng. 33, 1244–1259.

Hackley, P.C., Araujo, C.V., Borrego, A.G., Bouzinos, A., Cardott, B.J., Cook, A.C., Eble, C., Flores, D., Gentzis, T., Gonçalves, P.A., Mendonça Filho, J.G., Hámor-Vidó, M., Jelonek, I., Kommeren, K., Knowles, W., Kus, J., Mastalerz, M., Menezes, T. R., Newman, J., Oikonomopoulos, I.K., Pawlewicz, M., Pickel, W., Potter, J., Ranasinghe, P., Read, H., Reyes, J., Rosa Rodriguez, G.D.L., Alves Fernandes de Souza, I.V., Suárez-Ruiz, I., Sýkorová, I., Valentine, B.J., 2015. Standardization of reflectance measurements in dispersed organic matter: results of an exercise to improve interlaboratory agreement. Mar. Petrol. Geol. 59, 22–34.

Hakimi, M.H., Abdullah, W.H., Shalaby, M.R., 2010. Source rock characterization and oil generating potential of the Jurassic Madbi Formation, onshore East Shabowah oilfields, Republic of Yemen. Org. Geochem. 41, 513–521.

Hakimi, M.H., Ahmed, A., Kahal, A.Y., Hersi, O.S., Al Faifi, H.J., Qaysi, S., 2020. Organic geochemistry and basin modeling of Late Cretaceous Harshiyat Formation in the onshore and offshore basins in Yemen: implications for effective source rock potential and hydrocarbon generation. Mar. Petrol. Geol. 122.

Hakimi, M.H., Ahmed, A.F., 2016. Organic-geochemistry characterization of the Paleogene to Neogene source rocks in the Sayhut subbasin, Gulf of Aden Basin, with emphasis on organic-matter input and petroleum-generation potential. AAPG (Am. Assoc. Pet. Geol.) Bull. 100 (11), 1749–1774.

Hazra, B., Dutta, S., Kumar, S., 2017. TOC calculation of organic matter rich sediments using Rock-Eval pyrolysis: critical consideration and insights. Int. J. Coal Geol. 169, 106–115.

He, D.F., Zhang, L., Wu, S.T., Li, D., Zhen, Y., 2018. Tectonic evolution stages and features of the Junggar Basin. Oil Gas Geol. 39, 845–861.

He, J., Ding, W., Jiang, Z., Li, A., Wang, R., Sun, Y., 2016. Logging identification and characteristic analysis of the lacustrine organic-rich shale lithofacies: a case study from the Es3L shale in the Jiyang Depression, Bohai Bay Basin, Eastern China. J. Petrol. Sci. Eng. 145, 238–255.

Heroux, Y., Chagnon, A., Bertrand, R., 1979. Compilation and correlation of major thermal maturation indicators. AAPG (Am. Assoc. Pet. Geol.) Bull. 63, 2128–2144.

Hu, S., Zhao, W., Hou, L., Yang, Z., Zhu, R., Wu, S., Bai, B., Jin, X., 2020. Development potential and technical strategy of continental shale oil in China. Petrol. Explor. Dev. 47, 877–887.

Hu, T., Pang, X., Jiang, S., Wang, Q., Zheng, X., Ding, X., Zhao, Y., Zhu, C., Li, H., 2018. Oil content evaluation of lacustrine organic-rich shale with strong heterogeneity: a case study of the Middle Permian Lucaogou Formation in Jimusaer Sag, Junggar Basin, NW China. Fuel 221, 196–205.

Hu, T., Pang, X., Yu, S., Wang, X., Pang, H., Guo, J., Jiang, F., Shen, W., Wang, Q., Xu, J., 2016. Hydrocarbon generation and expulsion characteristics of Lower Permian P1f source rocks in the Fengcheng area, northwest margin, Junggar Basin, NW China: implications for tight oil accumulation potential assessment. Geol. J. 51, 880–900.

Hu, T., Pang, X.Q., Jiang, F.J., Wang, Q.F., Liu, X.H., Wang, Z., Jiang, S., Wu, G.Y., Li, C. J., Xu, T.W., Li, M.W., Yu, J.W., Zhang, C.X., 2021a. Movable oil content evaluation of lacustrine organic-rich shales: methods and a novel quantitative evaluation model. Earth Sci. Rev. 214.

Hu, T., Pang, X.Q., Jiang, F.J., Wang, Q.F., Wu, G.Y., Liu, X.H., Jiang, S., Li, C.R., Xu, T. W., Chen, Y.Y., 2021b. Key factors controlling shale oil enrichment in saline lacustrine rift basin: implications from two shale oil wells in Dongpu Depression, Bohai Bay Basin. Petrol. Sci. 18, 687–711.

Huang, H., Li, R., Chen, W., Chen, L., Jiang, Z., Xiong, F., Guan, W., Zhang, S., Tian, B., 2021. Revisiting movable fluid space in tight fine-grained reservoirs: a case study from Shahejie shale in the Bohai Bay Basin, NE China. J. Petrol. Sci. Eng. 207, 109170.

Huang, H., Li, R., Jiang, Z., Li, J., Chen, L., 2020a. Investigation of variation in shale gas adsorption capacity with burial depth: insights from the adsorption potential theory. J. Nat. Gas Sci. Eng. 73, 104344.

Huang, H., Li, R., Xiong, F., Hu, H., Sun, W., Jiang, Z., Chen, L., Wu, L., 2020b. A method to probe the pore-throat structure of tight reservoirs based on low-field NMR: insights from a cylindrical pore model. Mar. Petrol. Geol. 117, 104344.

Imin, A., Zha, M., Ding, X., Bian, B., Liu, Y., Zheng, M., Han, C., 2020. Identification of a Permian foreland basin in the western Junggar Basin (NW China) and its impact on hydrocarbon accumulation. J. Petrol. Sci. Eng. 187.

Jarvie, D., 2014. Components and processes affecting producibility and commerciality of shale resource systems. Geol. Acta: Int. Earth Sci. J. 12, 307–325.

Jarvie, D.M., 2012. Shale resource systems for oil and gas Part 2: shale-oil resource systems. In: Shale Reservoirs—Giant Resources for the 21st Century, vol. 97. AAPG Memoir, pp. 89–119.

Jiang, Y., Dong, D., Qi, L., Shen, Y., Jiang, C., He, F., 2010. Basic features and evaluation of shale gas reservoirs. Nat. Gas. Ind. 30 (10), 7–12.

Jin, H., Sonnenberg, S.A., Sarg, J.F., 2012. Source Rock Evaluation for the Bakken Petroleum System in the Williston Basin (North Dakota and Montana).

Jin, X., Li, G., Meng, S., Wang, X., Liu, C., Tao, J., Liu, H., 2021. Microscale comprehensive evaluation of continental shale oil recoverability. Petrol. Explor. Dev. 48, 256–268.

Katz, B., Lin, F., 2014. Lacustrine basin unconventional resource plays: key differences. Mar. Petrol. Geol. 56, 255–265.

Katz, B.J., Lin, F., 2021. Consideration of the limitations of thermal maturity with respect to vitrinite reflectance, Tmax, and other proxies. AAPG (Am. Assoc. Pet. Geol.) Bull. 105, 695–720.

Ko, L.T., Loucks, R.G., Zhang, T., Ruppel, S.C., Shao, D., 2016. Pore and pore network evolution of Upper Cretaceous Boquillas (Eagle Ford–equivalent) mudrocks: results from gold tube pyrolysis experiments. AAPG (Am. Assoc. Pet. Geol.) Bull. 100, 1693–1722.

Ko, L.T., Ruppel, S.C., Loucks, R.G., Hackley, P.C., Zhang, T., Shao, D.J., 2018. Pore-types and pore-network evolution in Upper Devonian-Lower Mississippian Woodford and Mississippian Barnett mudstones: insights from laboratory thermal maturation and organic petrology. I.J.O.C.G 190, 3–28.

Li, M., Chen, Z., Ma, X., Cao, T., Qian, M., Jiang, Q., Tao, G., Li, Z., Song, G., 2019. Shale oil resource potential and oil mobility characteristics of the eocene-oligocene Shahejie Formation, jiyang super-depression, bohai Bay basin of China. Int. J. Coal Geol. 204, 130–143.

Li, S., Hu, S., Xie, X., Lv, Q., Huang, X., Ye, J., 2016. Assessment of shale oil potential using a new free hydrocarbon index. Int. J. Coal Geol. 156, 74–85.

Li, W., Cao, J., Zhi, D., Tang, Y., He, W., Wang, T., Xia, L., 2021. Controls on shale oil accumulation in alkaline lacustrine settings: late Paleozoic Fengcheng Formation, northwestern Junggar Basin. Mar. Petrol. Geol. 129.

Liang, Y., Zhang, Y., Chen, S., Guo, Z., Tang, W., 2020. Controls of a strike-slip fault system on the tectonic inversion of the Mahu depression at the northwestern margin of the Junggar Basin, NW China. J. Asian Earth Sci. 198.

Liu, B., Wang, H., Fu, X., Bai, Y., Bai, L., Jia, M., He, B., 2019. Lithofacies and depositional setting of a highly prospective lacustrine shale oil succession from the Upper Cretaceous Qingshankou Formation in the Gulong sag, northern Songliao Basin, northeast China. AAPG (Am. Assoc. Pet. Geol.) Bull. 103, 405–432.

Liu, C., Xu, X., Liu, K., Bai, J., Liu, W., Chen, S., 2020. Pore-scale oil distribution in shales of the Qingshankou Formation in the changling sag, Songliao Basin, NE China. Mar. Petrol. Geol. 120.

Liu, G., Chen, Z., Wang, X., Gao, G., Xiang, B., Ren, J., Ma, W., 2016. Migration and accumulation of crude oils from Permian lacustrine source rocks to Triassic reservoirs in the Mahu depression of Junggar Basin, NW China: constraints from pyrrolic nitrogen compounds and fluid inclusion analysis. Org. Geochem. 101, 82–98.

Loucks, R.G., Reed, R.M., Ruppel, S.C., Hammes, U., 2012. Spectrum of pore types and networks in mudrocks and a descriptive classification for matrix-related mudrock pores. AAPG Bull. 96, 1071–1098.

Lu, S., Huang, W., Chen, F., Li, J., Wang, M., Xue, H., Wang, W., Cai, X., 2012. Classification and evaluation criteria of shale oil and gas resources: discussion and application. Petrol. Explor. Dev. 39, 268–276.
Makky, A.F., El Sayed, M.I., Abu El-Ata, A.S., Abd El-Gaied, I.M., Abdel-Fattah, M.I., Abd-Allah, Z.M., 2014. Source rock evaluation of some upper and lower cretaceous sequences, west beni suef concession, western desert, Egypt. Egypt. J. Petrol. 23, 135–149.
Marra, K.R., 2018. 2015 US geological survey assessment of undiscovered shale-gas and shale-oil resources of the mississippian Barnett shale, bend arch–fort worth basin, Texas. AAPG (Am. Assoc. Pet. Geol.) Bull. 102, 1299–1321.
Peters, K.E., 1986. Guidelines for evaluating petroleum source rock using programmed pyrolysis. AAPG (Am. Assoc. Pet. Geol.) Bull. 70, 318–329.
Peters, K.E., Hackley, P.C., Thomas, J.J., Pomerantz, A.E., 2018. Suppression of vitrinite reflectance by bitumen generated from liptinite during hydrous pyrolysis of artificial source rock. Org. Geochem. 125, 220–228.
Rickman, R., Mullen, M., Petre, E., Grieser, B., Kundert, D., 2008. A practical use of shale petrophysics for stimulation design optimization: all shale plays are not clones of the Barnett shale. In: SPE Annual Technical Conference & Exhibition.
Rybacki, E., Meier, T., Dresen, G., 2016. What controls the mechanical properties of shale rocks? – Part II: Brittleness. J. Petrol. Sci. Eng. 144, 39–58.
Salama, A.M., Abd-Allah, Z.M., El-Sayed, M.I., Elbastawesy, M.A., 2021. Source rock evaluation and burial history modeling of cretaceous rocks at the khalda concession of abu gharadig basin, western desert, Egypt. J. Afr. Earth Sci. 184.
Sanei, H., Petersen, H.I., Schovsbo, N.H., Jiang, C., Goodsite, M.E., 2014. Petrographic and geochemical composition of kerogen in the Furongian (U. Cambrian) Alum Shale, central Sweden: reflections on the petroleum generation potential. Int. J. Coal Geol. 132, 158–169.
Sonnenberg, S.A., H, J., Sarg, J.F., 2011. Bakken Mudrocks of the Williston Basin, World Class Source Rocks, AAPG Search and Discovery Article.
Tang, W., Zhang, Y., Pe-Piper, G., Piper, D.J.W., Guo, Z., Li, W., 2021. Permian to early Triassic tectono-sedimentary evolution of the Mahu sag, Junggar Basin, western China: sedimentological implications of the transition from rifting to tectonic inversion. Mar. Petrol. Geol. 123.
Tao, K., Cao, J., Chen, X., Nueraili, Z., Hu, W., Shi, C., 2019. Deep hydrocarbons in the northwestern Junggar Basin (NW China): geochemistry, origin, and implications for the oil vs. gas generation potential of post-mature saline lacustrine source rocks. Mar. Petrol. Geol. 109, 623–640.
Walton, I., McLe, J., 2013. The Role of Natural Fractures in Shale Gas Production, Effective and Sustainable Hydraulic Fracturing.
Wang, M., Wilkins, R.W.T., Song, G., Zhang, L., Xu, X., Li, Z., Chen, G., 2015. Geochemical and geological characteristics of the Es3L lacustrine shale in the Bonan sag, Bohai Bay Basin, China. Int. J. Coal Geol. 138, 16–29.
Wang, T., Cao, J., Jin, J., Xia, L., Xiang, B., Ma, W., Li, W., He, W., 2021. Spatiotemporal evolution of a late paleozoic alkaline lake in the Junggar Basin, China. Mar. Petrol. Geol. 124.
Wilson, M.J., Shaldybin, M.V., Wilson, L., 2016. Clay mineralogy and unconventional hydrocarbon shale reservoirs in the USA. I. Occurrence and interpretation of mixed-layer R3 ordered illite/smectite. Earth Sci. Rev. 158, 31–50.
Xia, L., Cao, J., Stüeken, E.E., Zhi, D., Wang, T., Li, W., 2020. Unsynchronized evolution of salinity and pH of a Permian alkaline lake influenced by hydrothermal fluids: a multi-proxy geochemical study. Chem. Geol. 541.
Yang, H., Chen, L., Kong, Y., 2004. A novel classification of structural units in Junggar Basin. Xinjing Pet. Geol. 25, 686–688.
Yu, K., Cao, Y., Qiu, L., Sun, P., 2018a. The hydrocarbon generation potential and migration in an alkaline evaporite basin: the Early Permian Fengcheng Formation in the Junggar Basin, northwestern China. Mar. Petrol. Geol. 98, 12–32.
Yu, K., Cao, Y., Qiu, L., Sun, P., 2019. Depositional environments in an arid, closed basin and their implications for oil and gas exploration: the lower Permian Fengcheng Formation in the Junggar Basin, China. AAPG (Am. Assoc. Pet. Geol.) Bull. 103, 2073–2115.
Yu, K., Cao, Y., Qiu, L., Sun, P., Jia, X., Wan, M., 2018b. Geochemical characteristics and origin of sodium carbonates in a closed alkaline basin: the lower permian Fengcheng Formation in the Mahu sag, northwestern Junggar Basin, China. Palaeogeogr. Palaeoclimatol. Palaeoecol. 511, 506–531.
Zhang, P., Misch, D., Hu, F., Kostoglou, N., Sachsenhofer, R.F., Liu, Z., Meng, Q., Bechtel, A., 2021a. Porosity evolution in organic matter-rich shales (Qingshankou Fm.; Songliao Basin, NE China): implications for shale oil retention. Mar. Petrol. Geol. 130.
Zhang, T., Fu, Q., Sun, X., Hackley, P.C., Ko, L.T., Shao, D., 2021b. Meter-scale lithofacies cycle and controls on variations in oil saturation, Wolfcamp A, Delaware and Midland Basins. AAPG (Am. Assoc. Pet. Geol.) Bull. 105, 1821–1846.
Zhang, Y., Li, W., Tang, W., 2018a. Tectonic setting and environment of alkaline lacustrine source rocks in the lower permian Fengcheng Formation of Mahu sag. Xinjing Pet. Geol. 39, 48–54.
Zhang, Z., Yuan, X., Wang, M., Zhou, C., Cheng, D., 2018b. Alkaline-lacustrine deposition and paleoenvironmental evolution in permian Fengcheng Formation at the Mahu sag, Junggar Basin, NW China. Petrol. Explor. Dev. 45, 1036–1049.
Zhao, W., Hu, S., Hou, L., Yang, T., Li, X., Guo, B., Yang, Z., 2020a. Types and resource potential of continental shale oil in China and its boundary with tight oil. Petrol. Explor. Dev. 47, 1–11.
Zhao, W., Zhang, B., Wang, X., Wu, S., Zhang, S., Liu, W., Wang, K., Zhao, X., 2021. Differences in source kitchens for lacustrine in-source and out-of-source hydrocarbon accumulations. Petrol. Explor. Dev. 48, 541–554.
Zhao, X., Pu, X., Zhou, L., Jin, F., Shi, Z., Han, W., Jiang, W., Zhang, W., 2020b. Typical geological characteristics and exploration practices of lacustrine shale oil: a case study of the Kong-2 member strata of the Cangdong Sag in the Bohai Bay Basin. Mar. Petrol. Geol. 113.
Zhi, D., Tang, Y., He, W., Guo, X., Zheng, M., Huang, L., 2021. Orderly coexistence and accumulation models of conventional and unconventional hydrocarbons in lower permian Fengcheng Formation, Mahu sag, Junggar Basin. Petrol. Explor. Dev. 48, 43–59.
Zhi, D., Tang, Y., Zheng, M., Xu, Y., Cao, J., Ding, J., Zhao, C., 2019. Geological characteristics and accumulation controlling factors of shale reservoirs in Fengcheng Formation, Mahu sag, Junggar Basin. China Petrol. Explor. 24, 615–623.
Zhou, L., Chen, C., Han, G., Yang, F., 2021. Difference characteristics between continental shale oil and tight oil and exploration practice: a case from huanghua depression, bohai Bay basin. Earth Sci. J. China Univ. Geosci. 46, 555–571.
Zou, C., 2012. Unconventional Petroleum Geology. Elsevier, Beijing.
Zou, C., Zhu, R., Chen, Z.-Q., Ogg, J.G., Wu, S., Dong, D., Qiu, Z., Wang, Y., Wang, L., Lin, S., Cui, J., Su, L., Yang, Z., 2019. Organic-matter-rich shales of China. Earth Sci. Rev. 189, 51–78.